Tuning of pK_as activates substrates in flavin-dependent aromatic hydroxylases

Warintra Pitsawong[1,#], Pirom Chenprakhon[2], Taweesak Dhammaraj[3], Dheeradhach Medhanavyn[4] , Jeerus Sucharitakul[5], Chanakan Tongsook[6], Willem J. H. van Berkel[7], Pimchai Chaiyen[8*], and Anne-Frances Miller[1*]

From the [1] Department of Chemistry, University of Kentucky, Lexington, KY, 40506-0055; [2] Institute for Innovative Learning, Mahidol University, Nakhon Pathom, 73170, Thailand; [3] Faculty of Pharmacy, Mahasarakham University, Thailand; [4] Department of Biochemistry and Center for Excellence in Protein and Enzyme Technology, Faculty of Science, Mahidol University, Bangkok, 10400, Thailand; [5] Department of Biochemistry, Faculty of Dentistry, Chulalongkorn University, Bangkok, 10300, Thailand; [6] Department of Chemistry, Faculty of Science, Silpakorn University, Nakhon Pathom, Thailand; [7] Laboratory of Food Chemistry, Wageningen University & Research, Bornse Weilanden 9, 6708 WG, Wageningen, The Netherlands; [8] School of Biomolecular Science and Engineering, Vidyasirimedhi Institute of Science and Technology, Wangchan Valley, 555 Moo 1 Payupnai, Wangchan, Rayong 21210 Thailand.

Running title: *Activation of bound substrates by deprotonation*

[#] Current address, Department of Biochemistry Brandeis University, Waltham, MA, 02453

*To whom correspondence should be addressed: Anne-Frances Miller, Department of Chemistry, University of Kentucky, Lexington, KY, 40506-0055, USA, Tel.: (859)-257-9349; Fax: (859)-323-1069, E-mail: afmill3r2@gmail.com and Pimchai Chaiyen, School of Biomolecular Science and Engineering Vidyasirimedhi Institute of Science and Technology (VISTEC), Wangchan Valley, 555 Moo 1 Payupnai, Wangchan, Rayong 21210 Thailand, Tel.: +66-2-201-5596 ; Fax: +66-2-354-7174 ; Email: pimchai.chaiyen@vistec.ac.th.

Keywords: flavin-dependent monooxygenase; ^{19}F NMR; pK_a tuning; NMR spectroscopy; Enzyme kinetics; Enzyme mechanism; flavin; flavoprotein.

ABSTRACT

Hydroxylation of substituted phenols by flavin-dependent monooxygenases is the first step of their biotransformation in various microorganisms. The reaction is thought to proceed via electrophilic aromatic substitution, catalyzed by enzymatic deprotonation of substrate, in single-component hydroxylases which use flavin as a cofactor (group A). However, two-component hydroxylases (group D), which use reduced flavin as a co-substrate, are less amenable to spectroscopic investigation. Herein, we employed ^{19}F-NMR in conjunction with fluorinated substrate analogs to directly measure pK_as and monitor protein events in hydroxylase active sites. We found that the single-component monooxygenase 3-hydroxybenzoate-6-hydroxylase (3HB6H) depresses the pK_a of bound substrate analog 4-fluoro 3-hydroxybenzoate (4F3HB) by 1.6 pH units, consistent with previously proposed mechanisms. The method was applied anaerobically to the two-component monooxygenase 4-hydroxyphenylacetate 3-hydroxylase (HPAH), revealing depression of the pK_a of 3-fluoro-4-hydroxyphenylacetate (3F4HPA) by 2.5 pH units upon binding to the C_2 component of HPAH. ^{19}F NMR also revealed a pK_a of 8.7 ± 0.05 that we attributed to an active site residue involved in deprotonating bound substrate, and assigned to His120 based on studies of protein variants. Thus, in both types of hydroxylases, we confirmed that binding favors the phenolate form of

substrate. The 9 kJ/mol and 14 kJ/mol magnitudes of the effects for 3HB6H and HPAH-C_2, respectively, are consistent with pK_a tuning by one or more H-bonding interactions. Our implementation of ^{19}F NMR in anaerobic samples is applicable to other two-component flavin-dependent hydroxylases and promises to expand our understanding of their catalytic mechanisms.

Hydroxylation of aromatic compounds is important in catabolism and transformation of xenobiotics for a wide variety of organisms. Such reactions are mostly catalyzed by metal-, pterin- and flavin-dependent enzymes (1-5). These enzymes also metabolize drugs and thereby modify their therapeutic effects (4). Enzymatic hydroxylation reactions are important for synthesis of fine chemicals and have been employed in various biocatalytic applications (6-10). The enzymes are able to activate molecular oxygen (O_2) and control the fate of the resulting reactive oxygen intermediate. Flavin-dependent monooxygenases catalyze aromatic hydroxylation by forming a reactive flavin-hydroperoxide adduct which can add a hydroxyl group to aromatic rings (11). Understanding how hydroxylases control the reactivity of activated O_2 is both fundamentally important and potentially valuable for improving the utility of hydroxylases for practical applications.

There are two broad categories of flavin-dependent aromatic hydroxylases: single component hydroxylases where flavin reduction and oxygenation occur on the same polypeptide chain, and two-component hydroxylases that require separate flavin reductase and substrate oxygenase components (11-13). Members of the first type utilize flavin as a cofactor, which remains bound throughout the catalytic cycle, whereas among the second type the oxygenase component binds reduced flavin as a substrate, and releases oxidized flavin as a product. Both types of hydroxylases catalyze the reaction of reduced flavin with O_2 to form a reactive C4a-hydroperoxyflavin intermediate (C4a-OOH) that reconciles the triplet nature of O_2 with the singlet substrates and products (14,15), and hydroxylates phenolic substrates (16).

For pyranose 2-oxidase and the oxygenase component (C_2) of HPAH, density functional theory (DFT) and transient kinetics indicate that reduced flavin reacts with O_2 via proton-coupled electron transfer to form a radical pair consisting of flavin semiquinone and •OOH radicals, before recombination of the radical pair to form the C4a-OOH hydroperoxyflavin adduct (17-19). Subsequent hydroxylation of phenolic substrates is thought to occur via electrophilic aromatic substitution, based on theoretical calculations (20), and because rates of hydroxylation are correlated with the favorability of flavin C4a-alkoxide formation, suggesting that this is a leaving group of the hydroxylation step (21,22). However, recent QM/MM calculations suggest that a hydroxyl radical coupled electron transfer mechanism applies in TropB (23).

Flavin-based hydroxylases are thought to activate their substrates for electrophilic attack by deprotonating them (24-30). Substrate binding to *para*-hydroxybenzoate hydroxylase appears to lower the substrate pK_a by approximately two pH units (27,29,31). Similarly, substrate is deprotonated upon binding to 3-hydroxybenzoate (3HB) 6-hydroxylase (3HB6H), wherein a nearby His residue is proposed to serve as the base (32). NMR studies found that substrate is (partially) deprotonated to the phenolate when bound to reduced phenol hydroxylase (33). Similarly, 2-methyl-3-hydroxypyridine-5-carboxylate oxygenase appears to preferentially bind its substrate as the zwitterionic form in which the phenol group is deprotonated (34). Thus, stabilization of bound phenolates is well established among single-component hydroxylases, and these therefore provide good systems in which to validate new methods for detecting and quantifying pK_a depression applied to substrate upon binding. However, novel approaches are sorely needed to investigate two-component hydroxylases.

Much less is known about two-component hydroxylases because they bind substrates when their flavin is reduced, and spectroscopically muted. Nevertheless, a low substrate pK_a was found to correlate with rapid hydroxylation by HadA (a dehalogenating monooxygenase), implying that substrate deprotonation is a rate-contributing step (35). Similarly, the phenolic pK_a of substrate bound to C_2 may be unusually low (Figure 1) since the hydroxylation rate constant and product yield are independent of pH from pH 6 to 10 (36). Active site mutants that preserve positive charge at the position of His120 retain activity consistent with a mechanism involving the phenolate form of substrate (37). However, quantitative studies of the

effect have yet to be performed, for lack of a method able to discern the protonation state of substrate when bound in the enzyme active site, while maintaining an inert atmosphere.

Ideally, one would like to know the pK_a of substrate in the presence of the flavin C4a-hydroperoxide, however the latter is very short-lived in the presence of substrate. As a proxy we have studied the $FMNH^-$-bound state of the C_2 oxygenase, in which we can assume that the enzyme has adopted the conformation in which formation and reaction of the hydroperoxide occurs.

In order to directly observe the influence of the active site environment on the pK_as of bound substrates, we used ^{19}F NMR. ^{19}F NMR provides high sensitivity comparable to ^1H NMR, but with superior responsiveness to changes in the environment as well as effects of deprotonation of the fluorinated molecule itself (38). Moreover, with ^{19}F incorporated only in the substrate analogs, the ^{19}F NMR spectra are not complicated by contributions from the protein or the buffer, so we could replicate conditions under which turnover could occur if O_2 were provided, without regard for the complexity of the ^1H spectra (Supporting Figure S1A). Although individual pK_as of the mono-fluorinated substrates are depressed somewhat by their fluorine substitutions, this should not greatly affect the *change* in pK_a associated with binding to enzyme. However, it is important to check that use of the analog does not result in mechanistic changes (39,40).

We validated the method by applying it to the fluorinated substrate 4F3HB that binds to the single-component hydroxylase 3HB6H. We then used it to characterize the state of the substrate 3F4HPA when bound to the C_2 component of HPAH. By using internal pH indicators monitored by ^1H NMR, we eliminated use of a pH electrode. This in turn enabled use of a septum-sealed anaerobic NMR tube and observation of the reduced ($FMNH^-$-bound) state of C_2, which is the state in which FMN binds to the protein (41). Because the NMR chemical shift indicators are small molecules they can easily be identified by their sharp lines despite the presence of equal or greater concentrations of protons from the protein (Supporting Figure S1A). This combination of ^{19}F NMR to observe the bound substrate, with ^1H NMR to measure the pH (Figure S1B), permits monitoring of pH titrations of bound (and free) ligand to test the hypothesis that the pK_a will be depressed upon binding to the enzyme.

The results indicate that the phenolate state of 4F3HB is stabilized by 1.6 pH units upon binding to 3HB6H, consistent with prior work (32). The method was then applied to a two-component hydroxylase, which proved more complicated. The dissociation constant describing 3F4HPA binding to C_2 was found to be strongly pH dependent consistent with preferential binding of the phenolate state to protonated protein and a pK_a of 6.49 for bound 3F4HPA. However, contributions from an additional ionization event attributable to the protein were also detected via ^{19}F chemical shifts, and tentatively assigned to an active site histidine via specific amino acid substitutions.

Thus, a single- and a two-component hydroxylase are unified mechanistically in that both deprotonate substrate as part of binding, and we have quantified the extent to which the deprotonated form is stabilized. Although much is known about single-component hydroxylases in this regard, two-component hydroxylases are less well documented. In this example, the exquisite sensitivity of the ^{19}F NMR chemical shift enabled us to observe deprotonation of substrate analogs and also to infer the occurrence of additional deprotonation events in the active site. This approach can have great value in additional members of this fascinating and useful enzyme family.

RESULTS

A single-component hydroxylase: pH dependence of 4F3HB alone – Before studying the fluorinated substrate (ligand) when bound to enzyme, we first characterized the free ligand to obtain a reference point. The ^{19}F chemical shift of 4F3HB dissolved in water was measured at 0.3 pH unit intervals from pH 2.0 to 12.0 and plotted as a function of pH (Figure 2). Two separate transitions could each be described by the Henderson-Hasselbalch equation (Eq. 3), yielding pK_as of 4.1 ± 0.01 and 8.7 ± 0.03 in excellent agreement with those obtained via titrations monitored by UV/Vis spectrophotometry (4.1 ± 0.05 and 8.5 ± 0.01, Supporting Figure S2, uncertainties quoted are errors of the fits). The identities of the events responsible for the pK_as were determined by ^{13}C NMR (Figure 2B).

To evaluate the extent to which the presence of a fluorine affects the pK_as, we also determined the

pK_as of authentic substrate, obtaining values of 4.2 ± 0.08 and 10.2 ± 0.08 (Figure S2) in agreement with literature (pK_{a1} = 4.0, pK_{a2} = 9.7 (32)). The carboxyl pK_a is thus relatively unaffected however the phenolic pK_a of the 4F3HB is 1.5 pH units lower than that of 3HB, consistent with electron withdrawal from the ring by the electronegative fluorine substituent (39). Our use of 4F3HB will therefore result in a lower phenolic pK_a relative to authentic substrate, but nonetheless provides an informative probe of effects of the 3HB6H active site on its bound substrate.

Crucially, these controls demonstrate ^{19}F NMR's ability to detect deprotonation of each of the compound's ionizable groups and distinguish between the two events (Figure 2A): deprotonation of the phenol group was associated with a small shift of the ^{19}F resonance to less negative chemical shift (0.32 ppm) whereas deprotonating the carboxyl group resulted in a large change in chemical shift to more negative values (-4 ppm). Thus the ^{19}F chemical shift displays a nuanced response not just to accumulating negative charge via the inductive effect, but also to interactions through space and ortho effects (42,43), producing an exquisitely responsive probe of local events (38).

pH dependence of the ^{19}F chemical shift of 4F3HB in the presence of wild-type 3HB6H – For 4F3HB in the presence of two-fold excess WT 3HB6H at pH 6.5 (Figure 3A), the ^{19}F resonance was shifted -0.20 ppm to more negative chemical shift relative to its position in the absence of enzyme, and was significantly broadened consistent with a larger correlation time for reorientation as part of a much larger entity (44).

The sample's pH was adjusted from 6.5 to 9.0 in small increments by repeated additions of 0.2 M KOH and from pH 10.0 back to 6.5 by additions of 1 M MES. At each point, the sample pH was determined from the ^{1}H chemical shifts of the indicator molecules, and the ^{19}F NMR spectrum of the ligand was collected. At pHs above pH 9.0, an additional sharper signal was observed (inset of Figure 3A). This was determined to be free 4F3HB by addition of excess 4F3HB to the enzyme solution, resulting in a single stronger sharp signal at an unchanged chemical shift. Appearance of free ligand was accompanied by protein precipitation, indicating that liberation of the ligand was due to protein denaturation rather than elevation of the dissociation constant (K_d). No further measurements were made on such samples.

A plot of the chemical shift of bound 4F3HB *vs.* pH and fitting with the Henderson-Hasselbalch equation (Eq. 3) yielded a pK_a of 7.1 ± 0.2 (Figure 3B). We attribute this to ionization of the phenolic OH because it is associated with a 0.27 ppm change to less negative chemical shift similar to the higher-pH ionization of free 4F3HB (Figure 3B, blue curve). Thus, binding to the enzyme depressed the phenolic pK_a of 4F3HB by 1.6 pH units relative to that of free 4F3HB (8.7 ± 0.03).

Binding of 4F3HB vs. pH – A binding site that lowers the ligand pK_a favors deprotonation of the ligand. Therefore, one predicts that the fluorinated analog with its intrinsically greater tendency to deprotonation should bind more readily than authentic substrate. Indeed, although 3HB's K_d of 0.05 - 0.16 mM for binding to 3HB6H (45,46) predicts that some 60 % of substrate would be protein-bound at the concentrations we used, the absence of any signal from free 4F3HB below pH 9.0 argues that this analog binds more tightly than does 3HB. This is consistent with 4F3HB's lower phenolic pK_a and preferential binding of the deprotonated phenolate form.

Having confirmed the expected behavior of a single-component hydroxylase using ^{19}F NMR, we applied the method to a two-component hydroxylase.

A two-component hydroxylase: 3F4HPA as a substrate for C_2 – As a model for the native substrate *p*-hydroxyphenylacetate (4HPA), we used 3F4HPA. This compound is itself a good substrate that reacts with the C_2 component in ways that resemble those of authentic substrate. Pre-steady-state kinetics of the reaction of reduced C_2 with a series of oxygen concentrations were examined by stopped-flow spectrophotometry. Absorbance changes at 380 and 450 nm (black and blue kinetic traces, respectively) revealed four phases for the reaction with 3F4HPA, similar to the reaction of C_2 with 4HPA (compare Figure 4 with Figure 5 in reference (41)). The first and second phases were dependent on the oxygen concentration, indicating that they reflect formation of a C4a-hydroperoxy-FMN intermediate.

The second-order rate constants of the first and second phases were calculated from the slopes of the plots of k_{obs} versus oxygen concentration, and found to be 1.16 x 10^6 $M^{-1}s^{-1}$ and 8.6 x 10^4 $M^{-1}s^{-1}$,

respectively. These are similar to the rate constants measured for the reaction of authentic substrate with C_2 (1.1 x 10^6 $M^{-1}s^{-1}$ and 4.8 x 10^4 $M^{-1}s^{-1}$ in the absence and presence of 4HPA, respectively (41)). Thus, presence of the fluorinated analog decreased the rate constant of C4a-hydroperoxy-FMN formation as does authentic substrate, and it appears that 3F4HPA, like 4HPA may crowd the active site and decrease O_2's access to reduced FMN (47). This further suggests that 3F4HPA binds in a position similar to that occupied by native substrate. Finally at high concentrations, 3F4HPA inhibited dehydration of C4a-hydroxy-FMN, similar to the effect of 4HPA (36) (Figure 4C). Thus, our pre-steady state characterizations affirm that 3F4HPA reproduces the environment and perturbations associated with bound substrate.

pH dependence of free 3F4HPA – As a reference point for our ^{19}F-NMR studies of 3F4HPA bound in to C_2, we measured the ^{19}F chemical shift of the free compound as a function of pH. Figure 5A shows two discrete transitions that were each described by the Henderson-Hasselbalch equation (Eq. 3) and yielded pK_as of 4.2 ± 0.04 and 9.0 ± 0.02, respectively, in excellent agreement with those obtained via UV/Vis spectrophotometry (4.0 ± 0.05 and 8.9 ± 0.01, respectively, Supporting Figure S3). Similar to the case of 4F3HB, the phenolic pK_a of 3F4HPA was 1.6 pH units lower than that of non-fluorinated substrate, while the carboxylic pK_a was much less affected (Supporting Figure S3A). As for 4F3HB, deprotonation of the *p*-hydroxyl group of 3F4HPA resulted in a small shift in the ^{19}F resonance to less negative chemical shifts, in contrast with the effect of deprotonating the acetic acid group.

pH dependence of the ^{19}F signal of 3F4HPA in the presence of wild-type HPAH-C_2 – To learn whether the pK_a of 3F4HPA is affected by interactions with the enzyme active site, we compared the pH dependence of bound 3F4HPA with that of free 3F4HPA. The pH of an NMR sample of 3F4HPA with 2.5-fold excess WT-C_2 and $FMNH^-$ was adjusted from 6.6 to 10.0 as described above, except that inert atmosphere was maintained. The highest pH investigated was pH 10.0 because C_2 denatures above this pH. The ^{19}F NMR spectrum exhibited a sharp signal from the unbound fraction at -139.312 ppm (pH 6.6) to -139.155 ppm (pH 10.0) in addition to a broad signal from the bound fraction at -137.959 (pH 6.6) to -139.692 ppm (pH 10.0) (Figure 6). At pH 6.6 the bound ligand ^{19}F chemical shift was 1.35 ppm less negative than that of the free ligand but in the course of the titration to high pH it moved to -0.54 ppm more negative in ^{19}F chemical shift relative to free ligand (pH 10.0). Thus, interaction with the protein had a significant effect on the ligand ^{19}F chemical shift and the effect had the opposite sign at high pH from at low pH, indicating that the nature of the interaction differs depending on the pH. This is in addition to, and different from, the effect of deprotonating the ligand, and therefore suggests an additional pH dependence residing in the protein.

The ^{19}F chemical shifts of bound and free 3F4HPA were plotted against pH (Figure 6B, black and blue, respectively). The pK_a values describing each were obtained from non-linear least-square fits using the Henderson-Hasselbalch equation (Eq. 3). Back-titration by addition of HCl gave the same results as those observed by addition of KOH indicating that the spectral changes were not due to increasing ionic strength in the course of the titrations nor an irreversible event such as protein denaturation. For free 3F4HPA, the chemical shift at each pH, the shape of the titration curve, and the pK_{LH} value of 8.9 ± 0.09 were within error of those associated with the deprotonation of the *p*-hydroxyl group of 3F4HPA in the absence of C_2 (9.0 ± 0.02) (Figure 5A).

The bound form of 3F4HPA behaved differently. The observed pK_a value of 8.7 ± 0.03 was similar to the pK_a of phenol deprotonation for free 3F4HPA, but the ^{19}F chemical shift change associated with the event was opposite in sign and much larger (-1.78 ppm vs +0.2 ppm for free 3F4HPA, δ_L - δ_{LH}). Indeed, the chemical shift change is more similar to the signature of deprotonating the carboxylic acid (Figure 5A).

We considered the possibilities that the pK_a of 8.7 represents (a) deprotonation of the bound ligand's phenol (as in 3HB6H), (b) deprotonation of the bound ligand's carboxyl (based on the chemical shift signature) or (c) response of the ligand ^{19}F chemical shift to deprotonation of a protein residue nearby ('X') (48). To arbitrate among the possibilities, we exploited the pH dependence of the apparent dissociation constant $K_{d,obs}$, as it provides an independent report on deprotonation events affecting the interaction between ligand and protein (Scheme 1). Because each of the pK_as of free ligand have been assigned, the pH dependence of $K_{d,obs}$ can

be used to test whether the pK_a of 8.7 reflects either pK_a of the bound ligand, where a given pK_a of free ligand is pK_{LH} and the corresponding pK_a of the bound ligand is p$K_{LH(EH)}$.

$$K_{d,obs}(pH) = K_{d,L\bullet EH}\frac{(1+10^{(pK_{LH}-pH)})}{(1+10^{(pK_{LH(EH)}-pH)})} \quad \text{(Eq. 1)}$$

Scheme 1 here please

Because binding of 3F4HPA to WT-C_2 increased as the pH increased (Figure 6A), we employ notation emphasizing binding of deprotonated ligand, which in turn will interact more favorably with positively charged (protonated) enzyme active site residue X. However, both protonation states of both groups are accounted for by the algebra employed below (Equations 4 and 5).

The predictions of scenarios (a) and (b) are plotted in Supplemental Figure S4 for comparison with the actual pH dependence of $K_{d,obs}$s. Neither are compatible with the data. Therefore, the simple model considering only the protonation state of the ligand is unable to account for the pK_a of 8.7 and we must adopt the model that it reflects a protein residue. Thus we now consider that there are two ionizable residues: the ligand phenol and X. This yields the expanded Scheme 2, which posits that the interaction will be favorable when the ligand is deprotonated and X is protonated (Supporting Figure S5). X's pK_a can then be extracted from the pH dependence of the chemical shift of bound ligand (p$K_{(L)EH}$ in Scheme 2), while the pK_a of the bound ligand's phenol can be extracted from the pH dependence of $K_{d,obs}$ (Equations 4 and 5).

Scheme 2 here please

Fits to the pH dependencies of the chemical shift of bound ligand $\delta_{obs}(pH)$, and the $K_{d,obs}(pH)$ indeed yielded two different pK_as. This is not unexpected; whereas the chemical shift of bound 3F4HPA only reflects the states in which ligand is bound, the $K_{d,obs}$ reflects equilibria with states of free ligand and free enzyme as well (Schemes 1 and 2, Eqs. 1 and 5).

A fit to the $K_{d,obs}$ data assuming only one labile proton (e.g. pK_as for ligand, bound and free, Eq. 1) and fixing the pK_a free ligand at pK_{LH} = 9.0 (above) displays systematic deviation from the data between pH 7.0 and 10.0 (orange dashed curve in Figure 7). Nevertheless it replicates the observed tighter binding at higher pH, with its convergence on a much lower p$K_{LH(EH)}$, and a lower pK_a for bound than for free ligand (6.7 ± 0.1, vs. 9.0 ± 0.02). Upon incorporating a second pK_a associated with X (Equation 5), the fit to data was excellent, replicating not only stronger binding at high pH, but also the biphasic behavior most evident near pH 8 (purple dotted curve in Figure 7). This lends credibility to our two-residues model (i.e. our assumption of 'EH' rather than 'E' at pH 7 and below). Again the fit yielded a considerably depressed p$K_{LH(EH)}$ = 6.3 ± 0.1, vs. pK_{LH} = 9.0, which was again fixed. Regardless of whether or not a second protonation event is considered, the p$K_{LH(EH)}$ value that emerges is consistent with promotion of substrate deprotonation upon binding to the enzyme. However, the two-residues fit yielded a pK_a of $pK_{(L)EH}$ = 8.1 ± 0.2 for the enzyme active site residue whereas the pK_a obtained by fitting the ^{19}F chemical shift of bound ligand using Eq. 3 is 8.77 ± 0.03 (teal curve in Figure 7).

Simultaneous fitting to both $\delta_{obs}(pH)$ and $K_{d,obs}(pH)$ provided good agreement with both (Figure 7, blue and red curves, respectively), although the fit to $K_{d,obs}(pH)$ is visibly inferior to the fit to $\delta_{obs}(pH)$. The simultaneous fit yielded a pK_a for bound ligand of p$K_{LH(EH)}$ of 6.49 ±0.09 (Table 2). The fact that similar values were obtained with different complexities of data sets and fits supports their validity. The 2.5 pH unit drop in ligand pK_a is consistent with stabilization of phenolate upon binding. The pK_a drop mirrors the 1.6 pH unit drop obtained for 4F3HB (above) although in the case of C_2 it was inferred via the pH dependence of $K_{d,obs}$ rather than that of δ_{obs}.

Because the simultaneous fit incorporates greater diversity and quantity of data, we adopt the parameters obtained from it as superior descriptors of the system. We emphasize that the model upon which they are based is not unique, and other solutions might be found that also fit our data. Nevertheless, the model in Scheme 2 has the virtues of being based on behavior also observed in 3HB6H, mechanistic studies of both enzymes, and residues known to be present in their active sites. In particular, the pK_{EH} value of 7.7 that emerges from the model and the data is compatible with X being a His residue.

pH dependence of the ^{19}F signal of 3F4HPA in the presence of C_2 variants H120N, H120R, and

S146A – We tested hypotheses for the identity of residue X by comparing our results on WT protein (above) with experiments on single-site variants. The crystal structure suggests that the conserved Ser146 and His120 are close to the ligand and could favor phenol deprotonation as indicated by the pH dependence of $K_{d,obs}$ (Figure 8B (49)). Analogues of C_2's His & Ser pair are found in other monooxygenase components, including those of cholesterol monooxygenase from *Mycobacterium tuberculosis* and chlorophenol 4-monooxygenase from *Burkholderia cepacia* (50,51). These residues have moreover been shown to affect the catalytic parameters and their dependence on pH (37).

To test the possibility that His120 is responsible for the pH-dependent environment sensed by bound 3F4HPA, we collected ^{19}F spectra of 3F4HPA in the presence of H120N- and H120R-C_2. These were chosen because the proteins are sufficiently stable for study by NMR, and because the H120R variant retains catalytic activity, albeit impaired (37). ^{19}F NMR spectra collected as for WT revealed only the free form of 3F4HPA in the presence of the H120N or H120R variants. This is consistent with the K_d value for binding of 4HPA to H120N:C4a-hydroperoxyflavin of 2.2 mM *versus* 0.18 mM for the analogous WT-C_2:C4a-hydroperoxyflavin complex (37). Thus, we confirm that His120 aids in binding 3F4HPA. However, we could not explore the possibility that His120 interacts directly with the F substituent of 3F4HPA.

As a control we also studied S146A-C_2 which eliminates an interaction with the phenol suggested by crystal structures (Figure 8B) (49). ^{19}F NMR spectroscopy revealed signals for both bound and free 3F4HPA, as for the WT-C_2. The plot of the ^{19}F chemical shift of bound 3F4HPA *versus* pH revealed a pK_a of 8.70 ± 0.08 associated with a more negative chemical shift upon deprotonation, as for WT-C_2 (Supporting Figure S6). Thus, we can rule out Ser146 as the source of the pK_a that affects bound ligand's chemical shift. Moreover, since Ser146 interacts with the ligand phenol this strengthens our conclusion that the pK_a of 8.7 is not due to the ligand phenol. This leaves His120 as the remaining reasonable source of the pK_a of 8.7, consistent with all the data in hand.

Single turnover reaction of wild-type C_2 with 3F4HPA at various pHs – To learn whether the protein residue with a pK_a of 8.7 affects reactivity of the F, we turned to product analyses. The F substituent of 3F4HPA results in the molecule not being symmetric about the 1-4 axis and creates the possibility of forming two different products depending on whether hydroxylation displaces the F at position 3 or hydroxylates at position 5 (see Jadan *et al*. (40) and Figure 8B). We hypothesized that the interaction affecting the ligand's ^{19}F chemical shift could also bias the binding orientation of 3F4HPA and produce a pH-dependent ratio of products.

Product yields on the order of 25% were obtained, possibly because the electron-withdrawing F substituent diminishes 3F4HPA's reactivity as a target for electrophilic attack. Interestingly, the distribution of products obtained did *not* change with pH, revealing F^- displacement in approximately 53% of the reactions and hydroxylation at position 5 in approximately 47%, over the pH range of 6.0 to 10.0 (Supplemental Table S1). Thus, 3F4HPA appears able to bind in either orientation (Figure 8B) and the absence of a a change centered at pH 8.7 indicates that interaction between ionizable residue X and the F in the $FMNH^-$ state does not greatly bias the branching ratio between the two reactions that can occur. This agrees with Peelen *et al.* who concluded that deprotonation of 3F-phenol in *Trichosporon cutaneum* phenol hydroxylase made the two *ortho* positions equally electron rich and therefore equally subject to attack, although there was a three-fold difference between them when substrate was protonated (33) (and see (52)). The pH-independent product ratio down to pH = 6.0 agrees with the pH independence of the hydroxylation rate in indicating that bound substrate's pK_a is significantly lower than 6.0 in the state of the enzyme in which reaction occurs.

The apparent discrepancy with our measured p$K_{LH(EH)}$ of 6.49 ± 0.09 can be because the reaction occurs in the presence of neutral C4a-hydroperoxyflavin, whereas the NMR studies were in the presence of anionic $FNMH^-$, the charge of which would tend to raise the pK_as of nearby residues.

DISCUSSION

Ionization state of ligand bound to 3HB6H and identities of residues affecting it– 3HB6H served as a test system for validating our ^{19}F NMR approach. The ^{19}F chemical shift of bound 4F3HB changed as expected for deprotonation of the phenol and

demonstrating a pK_a depressed from 8.7 to 7.1 upon binding to enzyme. This contrasts with the earlier finding that the UV spectrum of 3HB did not appear to change significantly upon binding to enzyme at pH 8.0, arguing against deprotonation (32). However, ^{19}F NMR provides a signal exclusive to the fluorinated ligand that is less subject to interference from other components of the sample (Supporting Figure S1). Our pK_a of 7.1 and ^{19}F NMR spectra at pHs near 8.0 concur that bound ligand is mostly deprotonated near pH 8.0 (Figure 3).

The current studies also demonstrate that replacement of His213 with Ser eliminates active site stabilization of the phenolate form of substrate. This is consistent with the larger K_d reported for 3HB binding of 0.72 mM for H213S, *vs*. the WT value of 0.15 mM (32) and can explain the lowered (28%) efficiency with which H213S-3HB6H produces product (*vs*. 86% for WT). Proton transfer from substrate to nearby His213 was proposed to produce a His^+•$phenolate^-$ pair in which substrate is activated for electrophilic attack (32). His213's Nε2 is 3 Å from the phenolic OH of one of the substrate poses found in the H213S structure (Figure 8A) (53). Moreover, His213 Nδ1 is 3 Å from Nε2 of another His, His363, which is itself polarized by a H-bond to the carbonyl O of Gly359. Thus, His213 appears to be supported by a relay of H-bonds that could prime it to abduct a proton from the substrate phenol (32), see also (53).

The crystal structures of 3HB6H also reveal a Cl^- ion bound against the flavin *re* face, consistent with inhibition of 3HB6H's reactions with O_2 and NADH by Cl^- (53), and the ability of Cl^- to act as a superoxide analog (54). Thus, we speculate that the Cl^- may identify the pocket in which the hydroperoxide functional group forms. Such a location would enable the distal OH of C4a-hydroperoxide to attack the substrate carbon *para* to the hydroxyl group when the latter is interacting with His213.

HPAH-C_2: Use of complementary observables to validate a model and extract pK_a values for ligand and protein events. – We exploited distinct ^{19}F signals from bound and free ligand to determine $K_{d,obs}$ as a function of pH. $K_{d,obs}$ reflects states of free enzyme and ligand as well as bound states, so $K_{d,obs}$ reports on ionization events additional to those affecting the ligand ^{19}F chemical shift. The pH dependence of $K_{d,obs}$ ruled out the ligand's own ionization events as sources of the pK_a of 8.7 affecting ligand chemical shift, so this pK_a was assigned to a protein residue 'X'. The resulting enlarged model (Scheme 2) explains the pH dependence of $K_{d,obs}$ substantially in terms of a pK_a for bound ligand of p$K_{LH(EH)}$ = 6.49, and also yields a pK_a value for X in the absence of ligand (pK_{EH}). Thus, we learned the pK_as of X when bound and free, as well as the pK_as of ligand when bound and free.

The 2.5 pH unit drop in 3F4HPA's pK_a upon binding to C_2 demonstrates that the enzyme stabilizes the ligand's phenolate state, thereby activating it for electrophilic attack. The magnitude of the pK_a shift corresponds to stabilization of the phenolate by 14 kJ/mol relative to the phenol. Similarly, the 1.6 pH unit shift in the pK_a of 4F3HB upon binding to 3HB6H represents 9.1 kJ/mol stabilization of the deprotonated form relative to the protonated form.

The energies in question can derive from H-bonds, electrostatic interactions with active site residues, and/or from effects of the polarity of the active site (34,55). For example, the active site Asp of α-lytic protease from *Lysobacter enzymogenes* has a pK_a below 1.5 representing a shift of almost 3 pH units, attributed to H-bonds with backbone amides and side chains of a His and a Ser (56). Similarly, a salt bridge between two Asp residues in ribonuclease H1 from *Escherichia coli* elevates the pK_a of one Asp to 6.1 and depresses the pK_a of the other to 2.6 (57) whereas in the β subunit of F1-ATPase from *Bacillus* PS-3 the active site Glu has pK_a of 6.8, representing a 2.5 pH unit elevation (58). Thus, there are ample precedents for the sizes of pK_a shifts we have measured (59), based on the same side chains as those found in C_2's active site (60).

Identities of residues affecting the ionization state of substrate bound to HPAH-C_2 – Residue X has a pK_a of 7.7 in our model, based on our data, making His120 the most plausible candidate. Crystal structures indicate that the side chain Nε of His120 is 3.0 Å from the hydroxyl group of 4HPA (Figure 8B) where it is well positioned to lower 4HPA's pK_a via a $N\varepsilon H^+$:$phenolate^-$ Coulomb interaction. Ser146 is also in position to donate a hydrogen bond (Figure 1). The flavin hydroquinone is nearby but is ruled out based on its pK_a of 6 or lower, inferred from the pH-independence of the rate of reaction with O_2 (36,61), Figure 8B).

Another His in the active site, His396, was determined to aid formation of the C4a-hydroperoxy-FMN (19), suggesting that His396's pK_a is above 10 due to the pH independence of the reaction rate between pH 6.3 and 9.9 (61). Thus, the viable candidates are Ser146 and His120. Because the event and its pK_a of 8.7 were retained when Ser146 is replaced by Ala, but ligand binding is lost when His120 is replaced, we identify X as His120.

Only C_2 variants with a positive charge at position 120 produced product (37), consistent with electrostatic stabilization of a phenolate substrate transition state. Finally, our pK_as of pK_{EH} = 7.7 and p$K_{(L)EH}$ = 8.7 are comparable to pK_as measured for other His residues. For example, the active site His in α-chymotrypsin from bovine pancreas has a pK_a of 7.5 that rises to ~10.3-12.1 upon binding of substrate analogs (62).

From an energetic standpoint, a protein-ligand interaction that stabilizes the anionic state of the ligand should conversely stabilize the cationic form of the binding site. Indeed, His120's pK_a is elevated when ligand is bound, from pK_{EH} = 7.7 to p$K_{(LH)EH}$ = 8.7. The magnitude of this change is only 1.0 pH unit, indicating that additional residues(s) contribute to the 2.5 pH unit depression of the ligand's pK_a. Based on its position (49) and conservation (50,51) Ser146 is an obvious candidate, and has been credited with positioning the substrate (37).

For S146A-C_2, the pH dependence of the ^{19}F chemical shift of bound ligand as well as its $K_{d,obs}$ yielded mostly similar parameters to those obtained for WT protein (compare Supporting Figure S6 with Figure 7). However pK_{EH} of His120 is 0.4 pH units lower in S146A-C_2 than in WT, compatible with a modest hydrogen bond between His120 and Ser146, and the p$K_{LH(EH)}$ of bound ligand is also lowered, to 4.8 *vs*. 6.49 for WT. Thus, it appears that Ser146 raises the pK_as of both His120 and bound substrate. The latter effect may be inconsequential because p$K_{LH(EH)}$ is quite low in WT and S146A, but elevation of His120's pK_{EH} to 7.7 can improve enzyme proficiency by extending the pH range over which the active site contains a cation. The effects of Ser146 are nevertheless small compared to the effect of the interaction between His120 and ligand, as p$K_{(L)EH}$ is unchanged at 8.7 in S146A-C_2.

Here too our results concur with the literature, as replacement of Ser146 by Ala barely changed the K_d (to 0.32 mM at pH 8.0, *vs* the WT K_d of 0.35 mM (41)), and S146A-C_2 can perform hydroxylation reasonably well (37), affirming a correlation between activity (36) and stabilization of the phenolate form of substrate demonstrated here.

Mechanistic implications of the residue ionization states that emerge – Our data support a model in which ligand binding to C_2 causes His120 to gain a proton at pHs between 7.7 and 8.7, while ligand loses one. In effect, a proton is transferred from ligand to His120 converting the two neutral functionalities to a counterion pair that stabilizes the anionic substrate (Figure 9). However the hydroxylation rate is pH-independent over a larger pH range, from 6.2 to 9.9 (36). This was thought to require that the p$K_{LH(EH)}$ of bound substrate be below 6.0 and the p$K_{(L)EH}$ of His120 with substrate bound be above 10. The current analysis finds that a His120 p$K_{(L)EH}$ higher than 8.7 is not necessary, because the ligand deprotonates without assistance from His120 at higher pHs, due to its p$K_{LH(E)}$ of 7.5 (Figure 9). Thus, the active site has the effect of stabilizing > 25% of deprotonated substrate from pH 6.0 up, whereas free substrate is >25% deprotonated only above pH 8.5.

At pHs near 6, we expect that the extent of substrate deprotonation would be greater in the state of the enzyme that actually undergoes reaction. We were constrained to study $FMNH^-$-containing enzyme whereas it is neutral C4a-hydroperoxy FMN participates in the rate-limiting step. The absence of anionic flavin in that case would tend to lower the pK_a of nearby ligand, explaining why our value for p$K_{LH(EH)}$ is higher than the pK_a < 6.0 determined from kinetics (36), despite our use of a fluorinated substrate.

Broader impact of the methodology – ^{19}F-containing substrate analogs in combination with the excellent responsiveness of ^{19}F's NMR chemical shift have afforded unique insight into the identities and energies of proton dissociation equilibria that contribute to the catalytic mechanisms of aromatic hydroxylases. There are prior examples of ^{19}F NMR of fluorinated ligands bound to enzymes (63), however ours stands out in having used both ^{19}F and ^{1}H spectra to determine ligand protonation state and pH in sealed samples that preserve the enzyme's redox state. Moreover, we combined the NMR with kinetic measurements to demonstrate that our ^{19}F probe is in fact a substrate. Our approach has wide applicability to diamagnetic aromatic

monooxygenases, flavin-based or not, and indeed to any enzymes for which fluorinated substrate analogs can be found and shown to mimic the behavior of authentic substrate. Because of ^{19}F's high gyromagnetic ratio, the NMR spectra are comparable in strength to ^{1}H spectra, so sub-mM concentrations of protein can be studied (38,64,65). However because ^{19}F is naturally absent from proteins, the spectra are uncomplicated by protein resonances or signals from most common buffers (Supporting Figure S1). Because the ^{19}F chemical shift is highly responsive to the environment (66) and there are very few distinct F atoms in the samples, the signals tend not to overlap. Thus simple one-dimensional (1D) NMR spectra suffice and the experiments can be applied to proteins too large for study by 2D and 3D NMR. Moreover the large chemical shift change associated with ligand binding means that faster on- and off-rates nonetheless remain in the slow-exchange limit providing separate bound and free signals.

In the case of C_2, an unexpected chemical shift signature and a large effect on the dissociation constant could both be explained on the basis of deprotonation of ligand in concert with a protein residue whose protonated form favors substrate binding. Thus ^{19}F NMR afforded information on a protein residue as well as the fluorinated ligand itself. It would be very interesting to apply this method to the reduced state of *para*-hydroxybenzoate hydroxylase where a pK_a of 7.1-7.4 has been assigned to bound substrate when the enzyme is oxidized based on UV data (27,29-31), but to His72 when the enzyme is reduced, despite a comparative dearth of data (67).

CONCLUSIONS

Our ^{19}F NMR studies demonstrate that the pK_a of substrate is depressed in both a single-component and a two-component flavoprotein hydroxylase, supporting deprotonation of the phenol group as a general mechanism of substrate activation for electrophilic attack among these enzymes. Several one-component oxygenases were known to bind substrate in phenolate form (30,31,33,34), but we now place this on quantitative footing, demonstrating 9.1 and 14 kJ/mol stabilization of substrate phenolate consistent with electrostatic or hydrogen bonding mechanisms.

The case of C_2 demonstrates the capacity of ^{19}F NMR to distinguish ligand deprotonation from other events, based on companion ^{13}C NMR experiments that identify specific deprotonation events (Figures 2 and 5). Thus, our data and model indicate that the protonation state of a nearby amino acid is coupled to that of the ligand. For both enzymes, comparisons with protein variants supported an active site His as substantially responsible for stabilizing bound ligand as the phenolate. In C_2, our experimentally-validated model supports formation of a His^+•$phenolate^-$ pair.

EXPERIMENTAL PROCEDURES

Materials – 3-fluoro-4-hydroxyphenylacetic acid (3F4HPA), 4-fluoro-3-hydroxybenzoic acid (4F3HB), maleic acid, and 4-methylimidazole (4-MI) were from Sigma-Aldrich. 2,4-dimethylimidazole (2,4-DMI) was from Lancaster Synthesis. Acetic acid was from EMD Millipore.

Enzymes – The genes for wild-type (WT) and variants of C_2 from *Acinetobacter baumanii* and 3HB6H from *Rhodococcus jostii* RHA1 were constructed and expressed, and proteins were purified as described previously (46,68,69)**.** Immediately before NMR data collection, enzymes were exchanged into 100 mM potassium chloride pH 6.0 by passage through a Sephadex™ G25 gel filtration chromatographic column equilibrated with 100 mM potassium chloride pH 6.0. The compounds used in the experiment (3F4HPA, 4F3HB, maleic acid, acetic acid, 4-MI, and 2,4-DMI) were dissolved in 100 mM potassium chloride to final concentrations of 10 mM and the resulting solutions were adjusted to pH ~6.0. The concentrations of the following compounds were determined using the known extinction coefficients: FMN, ε_{446} = 12.2 mM^{-1} cm^{-1}; FAD, ε_{450} = 11.3 mM^{-1} cm^{-1}, WT and all variants of C_2, ε_{280} = 56.7 mM^{-1} cm^{-1} (41); WT and all variants of 3HB6H, ε_{452} = 11.0 mM^{-1} cm^{-1} (46).

NMR Samples – NMR samples of WT and variants of C_2 were prepared under inert atmosphere in an anaerobic glove box (M-BRAUN UNIlab). The reduced holoenzyme solution (C_2:$FMNH^-$) was prepared by equilibration of 0.5 mM C_2 and 0.5 mM oxidized FMN with O_2-free atmosphere followed by reduction with a stoichiometric amount of sodium dithionite. Anaerobic solution of 3F4HPA was then added to yield a final concentration of 0.2 mM followed by addition of an aliquot of stock solution of NMR pH indicators (acetic acid, maleic acid, 4-MI, and 2,4-

DMI) to yield final concentrations of 1 mM, and sodium trimethylsilylpropanesulfonate (DSS) to yield a final concentration of 0.5 mM (internal chemical shift standard for ^{1}H). This solution was augmented with 25% (v/v) $^{2}H_2O$ for field locking and then 700 µL were transferred to a 5 mm NMR tube with a septum-lined screw cap (Wilmad CAT. #535-TR-7). A 1 mm capillary tube was filled with 0.1 mM potassium fluoride in 100 mM potassium chloride pH 6.0 to serve as a chemical shift reference for ^{19}F, and flame-sealed. This was placed in the NMR tube, which was then sealed before removal from the glove box.

For 3HB6H experiments, the NMR samples (aerobic condition) contained 0.8 mM of 3HB6H enzyme (in the oxidized state, WT or variants), 0.4 mM 4F3HB substrate analog, 1 mM indicators, 0.5 mM DSS, 0.1 mM KF (in a sealed capillary) and 25% $^{2}H_2O$ in 100 mM potassium chloride, pH 6.0. The provision of excess enzyme favored complete binding of the substrate analog.

NMR Spectroscopy – ^{19}F NMR spectra were acquired on a Varian INOVA 600 MHz NMR spectrometer using a 600 MHz ^{1}H-^{19}F/^{15}N-^{31}P 5mm PFG Switchable Probe with Z gradients, at 25 ºC (for WT and variants of C_2) or 4 ºC (for WT 3HB6H to accommodate the enzyme's moderate stability). The sample was equilibrated at each temperature for at least 30 min and the probe was tuned for detection of ^{19}F. After inserting the sample into the magnet bore, N_2 gas was used to maintain an inert atmosphere, control the temperature, maintain probe cooling, and spin NMR tubes at 20 Hz. ^{19}F spectra were obtained as 2.323 s acquisitions following a 90° excitation pulses (25 µs at 25 °C and 21.1 µs at 4 °C) separated by 3.9 s relaxation delays. A total of 6,400 transients were averaged per 28,000 Hz-wide 1D spectrum (total time ≈ 12 hours). Data were processed using 20 Hz Lorentz line-broadening prior to Fourier transformation. Chemical shift values were referenced to potassium fluoride in a capillary at -121 ppm. ^{19}F spectra of 4F3HB bound to 3HB6H were analyzed by Gaussian deconvolution using the software provided by the spectrometer manufacturer (VnmrJ 3.2) to yield the positions, widths and integrated areas of individual resonances, see Figure 3A.

^{1}H 1D NMR spectra were acquired on a Varian INOVA 400 MHz spectrometer using the 'Wet1D' pre-sequence with 300 Hz-wide on-resonance eburp1 waveforms to selectively excite the signal of bulk water in preparation for pulse-field gradient suppression, followed by a 90º excitation pulse to excite the full spectrum and a 1s acquisition time, with a 1s relaxation delay time between scans. The pH indicators' chemical shifts were tabulated relative to internal DSS at 0 ppm in 10000 Hz wide spectra produced by averaging 64 scans. Data were zero-filled once, weighted with a Gaussian or squared sine bell apodization function, and Fourier transformed.

^{13}C NMR spectra were obtained using a Varian INOVA 400 MHz spectrometer (100 MHz for ^{13}C) at 25 ºC. The sample solutions for ^{13}C NMR measurement were 0.1 M 3F4HPA, 10% $^{2}H_2O$, with $CDCl_3$ in a sealed capillary serving as an internal standard for ^{13}C, 77.23 ppm). The ^{13}C NMR spectra were obtained using a 45° excitation pulse, a 12 s delay between scans and proton decoupling throughout.

Calculation of the apparent dissociation constant, $K_{d,obs}$ – For the case of 3F4HPA binding to C_2, we calculated $K_{d,obs}$ at each pH based on the integrated peak areas of the bound and free forms of 3F4HPA. In the absence of chemical exchange, the 6.2 s interval we employed between 90° pulses would allow recovery of >95% and >93 % of bound and free ligand magnetization, respectively, based on the T_1 values of 2.25 ± 0.1 s for free 3F4HPA and $T_1 \leq$ 2 s for C_2 (calculated based on measurements for two other proteins and scaling for τ_c with the assumption that bound ligand tumbles with the protein (70)). The almost-complete recovery and similar degrees of saturation indicate that the two signals will similarly report on the concentration of the species they represent. Moreover taking into account chemical exchange employing the on-rate of 10 s^{-1} reported (41) or adjusted to the concentrations employed here (30 s^{-1}), simulations as per (71) show that the degree of saturation of the two ligands differs by less than 0.1 % with the 6.2 s recycle time we used.

The peak areas were used with knowledge that the total concentration of ligand was 0.2 mM to calculate bound and free ligand concentrations. Then the total enzyme concentration of 0.5 mM and the concentration of bound ligand (=ligand•enzyme complex, [LigEz]) was used to calculate the concentration of free enzyme, and thereby the dissociation constant in effect:

$$K_{d,obs} = \frac{[Lig]*(0.5-[LigEz])}{[LigEz]} \qquad \text{(Eq. 2)}$$

In this equation, the protonation states of the ligand and enzyme are not specified (this feature is incorporated below).

pH titrations – The internal NMR pH indicators with pK_a values spanning the range of 4.8 to 8.7 were chosen based on the simplicity of their spectra and non-interaction with the enzymes and their substrate binding. The pK_a of each of the indicators used was determined under our conditions (in 100 mM potassium chloride with 10% ^2H_2O and 0.5 mM DSS at 25°C) and the NMR response was documented, by withdrawing NMR samples at 0.3 pH unit intervals in a conventional pH electrode-monitored titration extending from pH 1 to 12. ^{1}H NMR spectra were acquired on a Varian INOVA 400 MHz as described above. The pK_a of each indicator was determined from plots of the indicators' chemical shifts versus the pH values provided by the electrode (Table 1). Thereafter, the known chemical shifts *vs*. pH were used to infer internal pH from the set of indicator chemical shifts without opening the sample to air or inserting a pH probe, because the indicators' chemical shift(s) vary with the pH near their pK_a (Figure S1).

For experiments on C_2, an anaerobic solution of potassium hydroxide (KOH) was titrated into 700 µL anaerobic NMR samples as described above. Each addition of KOH was made in an anaerobic glove box so the sample was never opened to air. Each 2 µL addition of 0.2 M KOH produced a ~0.3 pH unit change. After each KOH addition, a ^{1}H NMR spectrum was acquired at 400 MHz to determine the new pH and a ^{19}F NMR spectrum was acquired at 596 MHz (600 MHz for ^{1}H) to determine the 3F4HPA ^{19}F chemical shift. KCl (100 mM) was also present in the enzyme solution to minimize the change in overall ionic strength, and the reversibility of the titration was confirmed by addition of 0.1 M HCl to return the pH to its original range. Fewer points were taken from this back-titration because the enzyme is less amenable to addition of HCl. The ^{19}F chemical shifts *vs.* pH from the back-titration were compared with those obtained from the upward titration, and confirmed that titrations were reversible (Figures 3 and 6).

For 3HB6H experiments, titrations from pH 6.5 to 10.0 were accomplished by additions of aerobic 0.2 M KOH and the return to low pH was accomplished via additions of aerobic 1.0 M 2-(N-morpholino)ethanesulfonic acid (MES) *vide supra*. All titrations were performed at least twice.

Analysis of the pH dependence – The dissociation constants and chemical shifts measured at a series of pHs were modeled as functions of pH, with fitting to different models performed using KaleidaGraph (Synergy Software Version 4.5.3) and MatLab (Mathworks R2019a).

The pH dependence of the observed ^{19}F chemical shift δ_{obs} was modeled in terms of the Henderson-Hasselbalch equation:

$$\delta_{obs}(pH) = \frac{\delta_L\left(10^{(pH-pK_{LH})}\right)+\delta_{LH}}{\left(10^{(pH-pK_{LH})}\right)+1} \qquad \text{(Eq. 3)}$$

in which δ_{LH} and δ_L are the ^{19}F chemical shifts of the acid and base forms of the ligand (LH and L) and are the asymptotes obtained from the fit. The same equation was adapted to analyze absorbance as a function of pH.

Observed dissociation constants, $K_{d,obs}$, are understood to encompass multiple microscopic binding possibilities differing with respect to the protonation states of participating species. To shed light on these, the pH dependence of $K_{d,obs}$ was analyzed in terms of two different models.

1) In the first model, binding of ligand depends only on the protonation state of the ligand itself, and reflects pK_as of one proton in the enzyme-bound as well as the free state of the ligand $pK_{LH(EH)}$ and pK_{LH}, respectively (Scheme 1, 'EH' denotes enzyme in its protonated state). In our enzymes, tightest binding is attained for deprotonated ligand, L, so $K_{d,obs}(pH)$ is described relative to binding of L to EH: L + EH ⇔ L•EH.

2) In the second model, we additionally considered that the protonation state of an enzyme residue might also change in the pH range of interest (Scheme 2, the two-proton model, Equations 4, 5). The model incorporates interaction between the protonation states of the ligand (LH or L) and the enzyme (EH or E), where the species responsible for a pK_a is indicated in the subscript with the state of the other species, providing context in parentheses. Thus $pK_{LH(EH)}$ is the pK_a of ligand bound to the protonated state of the enzyme whereas $pK_{(L)EH}$ indicates the pK_a of the enzyme residue when deprotonated ligand is bound. Favorable interaction between a protonated

(cationic) enzyme residue and deprotonated (anionic) ligand will tend to raise the enzyme's pK_a and lower that of the ligand. Thus we expect that the ligand pK_a will decrease more upon binding to protonated enzyme than to deprotonated enzyme: p$K_{LH(EH)}$ < p$K_{LH(E)}$ and that bound ligand will display a pK_a of p$K_{LH(EH)}$ when the enzyme is protonated, i.e. when pH < $pK_{(L)EH}$.

$$\boldsymbol{\delta_{L,bound}(pH)} = \frac{\boldsymbol{\delta_{LE} + \delta_{LHE}10^{(pK_{LH(E)}-pH)} + \delta_{LEH}10^{(pK_{(L)EH}-pH)} + \delta_{LHEH}10^{(pK_{LH(EH)}+pK_{(L)EH}-2pH)}}}{\boldsymbol{1+10^{(pK_{LH(E)}-pH)} + 10^{(pK_{(L)EH}-pH)} + 10^{(pK_{LH(EH)}+pK_{(L)EH}-2pH)}}} \quad \text{(Eq. 4)}$$

and $\delta_{LHE} = \delta_{LE} - 0.15$, $\delta_{LEH} = \delta_{LHEH} + 0.15$, where 0.15 is the chemical shift change produced by ligand protonation, obtained from fits to data for free ligand.

$$\boldsymbol{K_{d,obs}(pH)} = \boldsymbol{K_{d,L\bullet EH}} \frac{\boldsymbol{\left(1+10^{(pK_{LH}-pH)}\right)\left(1+10^{(pH-pK_{EH})}\right)}}{\boldsymbol{\left(1+10^{(pK_{LH(EH)}-pH)} + 10^{(pH-pK_{(L)EH})}\left(1+10^{(pK_{LH(E)}-pH)}\right)\right)}} \quad \text{(Eq. 5)}$$

In the slow-exchange binding regime that applies to our systems, chemical shifts of bound ligand describe only the environment sensed by the bound population of ligand and reflect the protonation state of enzyme residues that interact with ligand as well as the protonation state of ligand itself (portion of Scheme 2 boxed in green). The $K_{d,obs}$ describes the equilibrium between all bound and all free ligand, and thus additionally reports on the pK_a of free ligand (pK_{LH}, known from titrations of free ligand) and free enzyme (pK_{EH}), in the portion of Scheme 2 boxed in red.

Details of fits – The pH dependence of the apparent dissociation constant $K_{d,obs}$ was fit with Equations 1 (model 1) and 5 (model 2) and the chemical shift of bound ligand was fit with Equation 3 or 4, respectively, to assess the merits of the different models and to extract parameters able to simultaneously describe both pH dependencies. Equations 4 and 5 together were used to fit a merged data set of δ_{obs} and $K_{d,obs}$ (Scheme 2).

Global fits to δ_{obs} and $K_{d,obs}$ were implemented in MatLab, wherein scaled chemical shifts (CS_{sc} = (δ_{obs} + 137.7)*5) were employed so that the magnitude of the total change would be 8.9, comparable to the total change of 9 for the $K_{d,obs}$. In fitting model 2 to the δ_{obs} of bound ligand *vs.* pH, we made the simplifying assumption that the chemical shift would respond similarly to the ligand's own protonation state when bound as when free, regardless of the protonation state of the protein residue. This allowed us to treat the difference $\delta_{L(EH)} - \delta_{LH(EH)}$ as equal to $\delta_{L(E)} - \delta_{LH(E)}$ and $\delta_L - \delta_{LH}$, of which the latter is known from titrations of free ligand. This decreased the number of unknown chemical shifts from 4 to 2, in the global fits. When pK_as obtained from these simplified fits were fixed and all four chemical shifts were optimized independently, the results did not change significantly.

Rapid kinetics experiments – Rapid kinetics measurements were performed with a Hi-Tech Scientific Model SF-61DX stopped-flow spectrophotometer in single-mixing and double-mixing modes. The optical path-length of the observation cell was 1 cm. The reactions were conducted at 4 °C. The stopped-flow instrument was made anaerobic by flushing with an oxygen-scrubbing solution consisting of 400 μM glucose, 1 mg/ml glucose oxidase (15.5 unit/ml) and 4.8 μg /ml catalase in 50 mM sodium phosphate buffer pH 7.0. The oxygen-scrubbing solution was allowed to stand in the flow system overnight and the system was thoroughly rinsed with anaerobic buffer before experiments were performed. To study the reaction of C_2 with oxygen, the reduced enzyme in the presence of substrate was prepared by rendering a solution of C_2 (100 μM) plus FMN (32 μM) anaerobic by equilibration in an anaerobic glove box, followed by stoichiometric reduction with sodium dithionite. The resulting solution was placed in a tonometer and transferred to the stopped-flow instrument. The reduced enzyme was mixed with buffers containing various oxygen concentrations (0.13, 0.31, 0.61 and 1.03 mM) and 2 mM 3F4HPA (41). All quoted concentrations are those obtained after mixing. Apparent rate constants (k_{obs}) were calculated from exponential

fits to the kinetic traces, performed using KineAsyst3 software (Hi-Tech Scientific, Salisbury, UK) or Program A (written at the university of Michigan by Rong Chang, Jung-yen Chiu, Joel Dinverno, and David P. Ballou). Rate constants were obtained by fitting plots of k_{obs} versus concentrations of oxygen with a Marquardt-Levenberg non-linear fit algorithm that is included in the KaleidaGraph software.

Single turnover reactions of wild-type C_2 with 3F4HPA at various pHs – 500 μL of an anaerobic solution of 200 μM C_2 with 100 μM $FMNH^-$ in 10 mM sodium phosphate buffer at pH 7.0 was mixed with an equal volume of 4.0 mM 3F4HPA in 100 mM buffer at 25 °C. After 15 min the reaction was quenched with 500 μL 0.15 M HCl. The experiment was repeated at a series of pHs by employing various pHs for the buffer of the 3F4HPA solution, including 100 mM sodium phosphate for pH 6.0 or 7.0, 100 mM Tris-HCl for pH 8.0, and 100 mM Gly-NaOH for pH 9.0 or 10.0. The quenched solutions were separated from the enzyme using Microcon® ultracentrifugal filters (10 kDa cut-off). The filtrates were analyzed using HPLC with diode array detection and mass spectrometry detection.

ACKNOWLEDGMENTS

Research reported in this publication was supported by the Vice President for Research of the University of Kentucky, the Center for Pharmaceutical Development (N.S.F. I/UCRC IIP-1540011 to A.-F.M.), a Research Challenge Trust Fund Fellowship (to W.P.), the National Sciences Foundation, Chemistry of Life Processes CHE-1808433 (A.-F.M.), the Thailand Science Research and Innovation Global Partnership Program and Vidyasirimedhi Institute of Science and Technology (VISTEC) (to P. Chaiyen), MRG6180156 (to P. Chenprakhon) and RSA5980062 (to J.S.). We thank A. Sebesta for repair of the anaerobic glove box.

CONFLICT OF INTEREST

The authors declare that they have no conflicts of interest with the contents of this article.

REFERENCES

1. van Berkel, W. J. H., Kamerbeek, N. M., and Fraaije, M. W. (2006) Flavoprotein monooxygenases, a diverse class of oxidative biocatalysts. *J. Biotechnol.* **124**, 670-689
2. Huijbers, M. M. E., Montersino, S., Westphal, A. H., Tischler, D., and van Berkel, W. J. H. (2014) Flavin dependent monooxygenases. *Arch. Biochem. Biophys.* **544**, 2-17
3. Torres Pazmiño, D. E., Winkler, M., Glieder, A., and Fraaije, M. W. (2010) Monooxygenases as biocatalysts: Classification, mechanistic aspects and biotechnological applications. *J. Biotechnol.* **146**, 9-24
4. Fagan, R. L., and Palfey, B. A. (2010) Flavin-dependent enzymes. in *Comprehensive Natural Products Chemistry II* (Begley, T. ed.), Elsevier, Oxford, UK. pp 37-114
5. Costas, M., Mehn, M. P., Jensen, M. P., and Que, L., Jr. (2004) Dioxygen activation at mononuclear nonheme iron active sites: Enzymes, models, and intermediates. *Chem. Rev.* **104**, 939-986
6. Dhammaraj, T., Phintha, A., Pinthong, C., Medhanavyn, D., Tinikul, R., Chenprakhon, P., Sucharitakul, J., Vardhanabhuti, N., C., J., and Chaiyen, P. (2015) p-Hydroxyphenylacetate 3-hydroxylase as a biocatalyst for the synthesis of trihydroxyphenolic acids. *ACS Catalysis* **5**, 4492-4502
7. Pinthong, C., Phoopraintra, P., Chantiwas, R., Pongtharangkul, T., Chenprakhon, P., and Chaiyen, P. (2017) Green and sustainable biocatalytic production of 3,4,5-trihydroxycinnamic acid from palm oil mill effluent. *Process Chem.* **63**, 122-129
8. Tinikul, R., Chenprakhon, P., Maenpuen, S., and Chaiyen, P. (2018) Biotransformation of plant-derived phenolic acids. *Biotechnol. J.* **13**, 1700632
9. Zhu, Y., Zhang, Q., Li, S., Lin, Q., Fu, P., Zhang, G., Zhang, H., Shi, R., Zhu, W., and Zhang, C. (2013) Insights into caerulomycin A biosynthesis: a two-component monooxygenase CrmH-catalyzed oxime formation. *J. Am. Chem. Soc.* **135**, 18750–18753
10. Baker Dockrey, S. A., Lukowski, A. L., Becker, M. R., and Narayan, A. R. H. (2018) Biocatalytic site- and enantioselective oxidative dearomatization of phenols. *Nat. Chem.* **10**, 119-125
11. Chenprakhon, P., Wongnate, T., and Chaiyen, P. (2019) Monooxygenation of aromatic compounds by flavin-dependent monooxygenases. *Protein Sci.* **28**, 8-29
12. Sucharitakul, J., Tinikul, R., and Chaiyen, P. (2014) Mechanisms of reduced flavin transfer in the two-component flavin-dependent monooxygenases. *Arch. Biochem. Biophys.* **555**, 33-46
13. Holtmann, D., and Hollmann, F. (2016) The oxygen dilemma: A severe challenge for the application of monooxygenases? *Chembiochem* **17**, 1391-1398
14. Massey, V. (1994) Activation of molecular oxygen by flavins and flavoproteins. *J. Biol. Chem.* **269**, 22459-22462
15. Eberlein, G., and Bruice, T. C. (1983) The chemistry of a 1,5-diblocked flavin. 2. Proton and electron transfer steps in the reaction of dihydroflavins with oxygen. *J. Am. Chem. Soc.* **105**, 6685–6697
16. Mattevi, A. (2006) To be or not to be an oxidase: challenging the oxygen reactivity of flavoenzymes. *Trends Biochem. Sci.* **31**, 276–283

17. Wongnate, T., Surawatanawong, P., Visitsatthawong, S., Sucharitakul, J., Scrutton, N. S., and Chaiyen, P. (2014) Proton-coupled electron transfer and adduct configuration are important for C4a-hydroperoxyflavin formation and stabilization in a flavoenzyme. *J. Am. Chem. Soc.* **136**, 241-253
18. Chenprakhon, P., Trisrivirat, D., Thotsaporn, K., Sucharitakul, J., and Chaiyen, P. (2014) Control of C4a-hydroperoxyflavin protonation in the oxygenase component of *p*-hydroxyphenylacetate-3-hydroxylase. *Biochemistry* **53**, 4084-4086
19. Visitsatthawong, S., Chenprakhon, P., Chaiyen, P., and Surawatanawong, P. (2015) Mechanism of oxygen activation in a flavin-dependent monooxygenase: A nearly barrierless formation of C4a- hydroperoxyflavin via proton-coupled electron transfer. *J. Am. Chem. Soc.* **137**, 9363-9374
20. Ridder, L., Harvey, J. N., Rietjens, I. M. C. M., Vervoort, J., and Mulholland, A. J. (2003) Ab initio QM/MM modeling of the hydroxylation step in *p*-hydroxybenzoate hydroxylase. *J. Phys. Chem. B* **107**, 2118–2126
21. Ortiz-Maldonado, M., Ballou, D. P., and Massey, V. (1999) Use of free energy relationships to probe the individual steps of hydroxylation of *p*-hydroxybenzoate hydroxylase: studies with a series of 8-substituted flavins. *Biochemistry* **38**, 8124-8137
22. Chaiyen, P., Sucharitakul, J., Svasti, J., Entsch, B., Massey, V., and Ballou, D. P. (2004) Use of 8-substituted-FAD analogues to investigate the hydroxylation mechanism of the flavoprotein 2-methyl-3-hydroxypyridine-5-carboxylic acid oxygenase. *Biochemistry* **43**, 3933-3943
23. Tweedy, S. E., Benítez, A. R., Narayan, A. R. H., Zimmerman, P. M., Brooks, C. L., III., and Wymore, T. (2019) Hydroxyl radical-coupled electron-transfer mechanism of flavin-dependent hydroxylases. *J. Phys. Chem. B* **123**, 8065-8073
24. Wang, X., Hou, Q., and Liu, Y. (2018) Insights into the decarboxylative hydroxylation of salicylate catalyzed by the flavin-dependent monooxygenase salicylate hydroxylase. *Theor. Chem. Acc.* **137**, 89
25. Ridder, L., Mulholland, A. J., Rietjens, I. M. C. M., and Vervoort, J. (2000) A quantum mechanical/molecular mechanical study of the hydroxylation of phenol and halogenated derivatives by phenol hydroxylase. *J. Am. Chem. Soc.* **122**, 8728–8738
26. van Berkel, W. J. H., and Müller, F. (1989) The temperature and pH dependence of some properties of *p*-hydroxybenzoate hydroxylase from *Pseudomonas fluorescens*. *Eur. J. Biochem.* **179**, 307-314
27. Entsch, B., Palfey, B. A., Ballou, D. P., and Massey, V. (1991) Catalytic function of tyrosine residues in para-hydroxybenzoate hydroxylase as determined by the study of site-directed mutants. *J. Biol. Chem.* **266**, 17341-17349
28. Entsch, B., and van Berkel, W. J. H. (1995) Structure and mechanism of *para*-hydroxybenzoate hydroxylase. *FASEB J.* **9**, 476-483
29. Eschrich, K., van der Bolt, F. J. T., de Kok, A., and van Berkel, W. J. H. (1993) Role of Tyr201 and Tyr385 in substrate activation by *p*-hydroxybenzoate hydroxylase from *Pseudomonas fluorescens*. *Eur. J. Biochem.* **216**, 137-146
30. Benítez, A. R., Tweedy, S. E., Baker Dockrey, S. A., Lukowski, A. L., Wymore, T., Khare, D., Brooks, C. L., III., Palfey, B., A,, Smith, J. L., and Narayan, A. R. H. (2019) Structural basis

for selectivity in flavin-dependent monooxygenase-catalyzed oxidative dearomatization. *ACS Catalysis* **9**, 3633-3640

31. Shoun, H., Beppu, T., and Arima, K. (1979) On the stable enzyme•substrate complex of *p*-hydroxybenzoate hydroxylase. *J. Biol. Chem.* **254**, 899-904
32. Sucharitakul, J., Medhanavyn, D., Pakotiprapha, D., van Berkel, W. J. H., and Chaiyen, P. (2016) Tyr217 and His213 are important for substrate binding and hydroxylation of 3-hydroxybenzoate 6-hydroxylase from *Rhodococcus jostii* RHA1. *FEBS J.* **283**, 860-881
33. Peelen, S., Rietjens, I. M. C. M., van Berkel, W. J.H., van Workum, W. A., and Vervoort, J. (1993) ^{19}F-NMR study on the pH-dependent regioselectivity and rate of the *ortho*-hydroxylation of 3-fluorophenol by phenol hydroxylase from *Trichosporon cutaneum*. *Eur. J. Biochem.* **218**, 345-353
34. Chaiyen, P., Brissette, P., Ballou, D. P., and Massey, V. (1997) Reaction of 2-methyl-3-hydroxypyridine-5-carboxylic acid (MHCP) oxygenase with N-methyl-5-hydroxynicotinic acid: studies on the mode of binding, and protonation status of substrate. *Biochemistry* **36**, 13856-13864
35. Pimviriyakul, P., Surawatanawong, P., and Chaiyen, P. (2018) Oxidative dehalogenation and denitration by a flavin- dependent monooxygenase is controlled by substrate deprotonation. *Chem. Sci.* **9**, 7468–7482
36. Ruangchan, N., Tongsook, C., Sucharitakul, J., and Chaiyen, P. (2011) pH-dependent studies reveal an efficient hydroxylation mechanism of the oxygenase component of *p*-hydroxyphenylacetate 3-hydroxylase. *J. Biol. Chem.* **286**, 223-233
37. Tongsook, C., Sucharitakul, J., Thotsaporn, K., and Chaiyen, P. (2011) Interactions with the substrate phenolic group are essential for hydroxylation by the oxygenase component of *p*-hydroxyphenylacetate 3-hydroxylase. *J. Biol. Chem.* **286**, 44491-44502
38. Kitevski-LeBlanc, J. L., and Prosser, R. S. (2012) Current applications of ^{19}F NMR to studies of protein structure and dynamics. *Prog. Nucl. Magn. Reson. Spec.* **62**, 1-33
39. Husain, M., Entsch, B., Ballou, D. P., Massey, V., and Chapman, P. J. (1980) Fluoride elimination from substrates in hydroxylation reactions catalyzed by *p*-hydroxybenzoate hydroxylase. *J. Biol. Chem.* **255**, 4189-4197
40. Jadan, A. P., Moonen, M. J. H., Boeren, S., Golovleva, L. A., Rietjens, I. M. C. M., and van Berkel, W. J. H. (2004) Biocatalytic potential of *p*-hydroxybenzoate hydroxylase from *Rhodococcus rhodnii* 135 and *Rhodococcus opacus* 557. *Adv. Synth. Catal.* **346**, 367-375
41. Sucharitakul, J., Chaiyen, P., Entsch, B., and Ballou, D. P. (2006) Kinetic mechanisms of the oxygenase from a two-component enzyme, *p*-hydroxyphenylacetate 3-hydroxylase from *Acinetobacter baumannii*. *J. Biol. Chem.* **281**, 17044-17053
42. Sanders, L. K., and Oldfield, E. (2001) Theoretical investigation of ^{19}F NMR chemical shielding tensors in fluorobenzenes. *J. Phys. Chem. A* **105**, 8098-8104
43. Arunima, and Kurur, N. D. (2005) Ortho effect in fluorobenzenes: cross-correlated relaxation and quantum chemical studies. *Magn. Reson. Chem.* **43**, 132-138
44. Gerig, J. T. (2003) Fluorine NMR. in *Biophysics Textbook Online* (Society, B. ed.), Biophysical Society, Bethesda MD. pp 1-35
45. Montersino, S., and van Berkel, W. J. H. (2012) Functional annotation and characterization of 3-hydroxybenzoate 6-hydroxylase from *Rhodococcus jostii* RHA1. *Biochim. Biophys. Acta* **1824**, 433-442

46. Sucharitakul, J., Wongnate, T., Montersino, S., van Berkel, W. J. H., and Chaiyen, P. (2012) Reduction kinetics of 3-hydroxybenzoate 6-hydroxylase from *Rhodococcus jostii* RHA1. *Biochemistry* **51**, 4309-4321
47. Baron, R., Riley, C., Chenprakhon, P., Thotsaporn, K., Winter, R. T., Alfieri, A., Forneris, F., van Berkel, W. J. H., Chaiyen, P., Fraaije, M. W., Mattevi, A., and McCammon, J. A. (2009) Multiple pathways guide oxygen diffusion into flavoenzyme active sites. *Proc. Natl. Acad. Sci. U. S. A.* **106**, 10603-10608
48. Kahyaoglu, A., and Jordan, F. (2002) Direct proton magnetic resonance determination of the p*Ka* of the active center histidine in thiolsubtilisin. *Protein Sci.* **11**, 965-973
49. Alfieri, A., Fersini, F., Ruangchan, N., Prongjit, M., Chaiyen, P., and Mattevi, A. (2007) Structure of the monooxygenase component of a two-component flavoprotein monooxygenase. *Proc. Natl. Acad. Sci. U. S. A.* **104**, 1177-1182
50. Dresen, C., Lin, L. Y., D'Angelo, I., Tocheva, E. I., Strynadka, N., and Eltis, L. D. (2010) A flavin-dependent monooxygenase from *Mycobacterium tuberculosis* involved in cholesterol catabolism. *J. Biol. Chem.* **285**, 22264-22275
51. Webb, B. N., Ballinger, J. W., Kim, E., Belchik, S. M., Lam, K. S., Youn, B., Nissen, M. S., Xun, L., and Kang, C. (2010) Characterization of chlorophenol 4-monooxygenase (TftD) and NADH:FAD oxidoreductase (TftC) of *Burkholderia cepacia* AC1100. *J. Biol. Chem.* **285**, 2014-2027
52. Vervoort, J., Rietjens, I. M. C. M., van Berkel, W. J. H., and Veeger, C. (1992) Frontier orbital study on the 4-hydroxybenzoate-3-hydroxylase-dependent activity with benzoate derivatives. *Eur. J. Biochem.* **206**, 479-484
53. Montersino, S., Orru, R., Barendregt, A., Westphal, A. H., van Duijn, E., Mattevi, A., and van Berkel, W. J. H. (2013) Crystal structure of 3-hydroxybenzoate 6-hydroxylase uncovers lipid-assisted flavoprotein strategy for regioselective aromatic hydroxylation. *J. Biol. Chem.* **288**, 26235-26245
54. Kommoju, P.-R., Chen, Z., Bruckner, R. C., Mathews, F. S., and Jorns, M. S. (2011) Probing oxygen activation sites in two flavoprotein oxidases using chloride as an oxygen surrogate. *Biochemistry* **50**, 5521-5534
55. Isom, D. G., Castañeda, C. A., Cannon, B. R., and Garcia-Moreno, B. E. (2011) Large shifts in pK_a values of lysine residues buried inside a protein. *Proc. Natl. Acad. Sci. U S A* **108**, 5260-5265
56. Everill, P., Sudmeier, J. L., and Bachovchin, W. W. (2012) Direct NMR observation and pK_a determination of the Asp(102) side chain in a serine protease. *J. Am. Chem. Soc.* **134**, 2348-2354
57. Oda, Y., Yamazaki, T., Nagayama, K., Kanaya, S., Kuroda, Y., and Nakamura, H. (1994) Individual ionization-constants of all the carboxyl groups in ribonuclease HI from *Escherichia coli* determined by NMR. *Biochemistry* **33**, 5275-5284
58. Tozawa, K., Ohbuchi, H., Yagi, H., Amano, T., Matsui, T., Yoshida, M., and Akutsu, H. (1996) Unusual pK_a of the carboxylate at the putative catalytic position of thermophilic F-1-ATPase beta subunit determined by C-13-NMR. *Febs Lett.* **397**, 122-126
59. Fersht, A. (1985) *Enzyme Structure and Mechanism*, 2 ed., Freeman & Company, London

60. Anderson, D. E., Becktel, W. J., and Dahlquist, F. W. (1990) pH-induced denaturation of proteins: A single salt bridge contributes 3-5 kcal/mol to the free energy of folding of T4 lysozyme. *Biochemistry* **29**, 2403-2408
61. Thotsaporn, K., Chenprakhon, P., Sucharitakul, J., Mattevi, A., and Chaiyen, P. (2011) Stabilization of C4a-hydroperoxyflavin in a two-component flavin-dependent monooxygenase Is achieved through interactions at flavin N5 and C4a atoms. *J. Biol. Chem.* **286**, 28170-28180
62. Lin, J., Cassidy, C. S., and Frey, P. A. (1998) Correlations of the basicity of His 57 with transition state analogue binding, substrate reactivity, and the strength of the low-barrier hydrogen bond in chymotrypsin. *Biochemistry* **37**, 11940-11948
63. Dugad, L. B., and Gerig, J. T. (1988) NMR studies of carbonic anhydrase-4-fluorobenzenesulfonamide complexes. *Biochemistry* **27**, 4310-4316
64. Salopek-Sondi, B., and Luck, L. A. (2002) ^{19}F NMR study of the leucine-specific binding protein of *Escherichia coli*: mutagenesis and assignment of the 5-fluorotryptophan-labeled residues. *Prot. Eng.* **15**, 855-859
65. Stockman, B. J. (2008) 2-fluoro-ATP as a versatile tool for ^{19}F NMR-based activity screening. *J. Am. Chem. Soc.* **130**, 5870-5871
66. Gerig, J. T. (1994) Fluorine NMR of proteins. *Prog. NMR. Spec.* **26**, 293-370
67. Palfey, B. A., Moran, G. R., Entsch, B., Ballou, D. P., and Massey, V. (1999) Substrate recognition by "password" in *p*-hydroxybenzoate hydroxylase. *Biochemistry* **38**, 1153-1158
68. Chaiyen, P., Suadee, C., and Wilairat, P. (2001) A novel two-protein component flavoprotein hydroxylase - *p*-hydroxyphenylacetate hydroxylase from *Acinetobacter baumannii*. *Eur. J. Biochem.* **268**, 5550-5561
69. Thotsaporn, K., Sucharitakul, J., Wongratana, J., Suadee, C., and Chaiyen, P. (2004) Cloning and expression of *p*-hydroxyphenylacetate 3-hydroxylase from *Acinetobacter baumannii*: evidence of the divergence of enzymes in the class of two-protein component aromatic hydroxylases. *Biochim. Biophys. Acta* **1680**, 60-66
70. Ernst, R. W., and Anderson, W. A. (1966) Application of Fourier transform spectroscopy to magnetic resonance. *Rev. Sci. Instrum.* **37**, 93-102
71. Spencer, R. G. S., and Fishbein, K. W. (2000) Measurement of spin-lattice relaxation times and concentrations in systems with chemical exchange using the one-pulse sequence: Breakdown of the Ernst mode for partial saturation in nuclear magnetic resonance. *J. Magn. Reson.* **142**, 120-135
72. Perrin, D. D., and Dempsey, B. (1983) *Buffers for pH and Metal Ion Control*, Chapman and Hall, London
73. Valcour, A. A., and Woodworth, R. C. (1986) Internal proton magnetic resonance probes for pH titration of proteins. *J. Magn. Reson.* **66**, 536-541
74. Dhammaraj, T., Pinthong, C., Visitsatthwong, S., Tongsook, C., and Surawatanawong, P. (2016) A single-site mutation at Ser146 expands the reactivity of the oxygenase component of *p*-hydroxyphenylacetate 3-hydroxylase. *ACS Chem. Biol.* **11**, 2889-2896
75. Pettersen, E. F., Goddard, T. D., Huang, C. C., Couch, G. S., Greenblatt, D. M., Meng, E. C., and Ferrin, T. E. (2004) UCSF Chimera - a visualization system for exploratory research and analysis. *J. Comput. Chem.* **25**, 1605-1612

FOOTNOTES

1. Abbreviations

3,4-DHPA, 3,4-dihydroxyphenylacetate; 3-F-4,5-DHPA, 3-fluoro-4,5-dihydroxyphenylacetate; 3F4HPA, 3-fluoro-4-hydroxyphenylacetate; 3HB, 3-hydroxybenzoate; 3HB6H, 3-hydroxybenzoate-6-hydroxylase; 4F3HB, 4-fluoro 3-hydroxybenzoate; C_2, oxygenase component of *p*-hydroxyphenylacetate 3-hydroxylase; DFT Density functional theory; DSS, 2,2-dimethyl-2-silapentane-5-sulfonic acid; HPAH, *p*-hydroxyphenylacetate 3-hydroxylase; 4HPA, 4-hydroxyphenylacetate = *p*-hydroxyphenylacetate.

TABLES

TABLE 1. List of pH indicators used in the experiment.

Indicator Compound	**Resonance Observed**	**Resonance (ppm)**[a]	**Measured pK_a**[b]	**Literature pK_a**[c]
acetic acid	methyl proton	1.90-2.09	4.78 ± 0.08	4.76
maleic acid	C(2) proton	6.00-6.34	6.08 ± 0.03	6.26[d]
4-methylimidazole	C(2) proton	7.63-8.51	7.87 ± 0.0	7.52
	C(5) proton	6.82-7.15	7.89 ± 0.03	7.52
	C(4) methyl protons	2.19-2.33	7.86 ± 0.07	7.52
2,4-dimethylimidazole	C(5) proton	6.65-6.95	8.70 ± 0.06	8.64[e]
	C(2) methyl protons	2.30-2.55	8.67 ± 0.08	8.64[e]
	C(4) methyl protons	2.13-2.25	8.68 ± 0.08	8.64

[a] *vs.* vs. internal 0.5 mM DSS (chemical shift reference for ^{1}H)
[b] pK_as were determined in 10% ^2H_2O, 0.5 mM DSS, with 100 mM potassium chloride. Values are the averages of two independent measurements. An additional error may be contributed by the electrode.
[c] from Perrin and Dempsey (72), except where noted.
[d] the higher one of maleic acid's two pK_as, called pK_a^2 by Perrin and Dempsey (72).
[e] determined in 100% ^2H_2O with 100 mM potassium chloride at 25°C (73).

TABLE 2. Summary of pK_as observed and proposed chemical events associated with them.

	pK_a	**Observed Change in ^{19}F**	**Proposed Dissociating Proton**
4F3HB (without 3HB6H)	8.7 ± 0.03 (NMR) 8.5 ± 0.01 (UV/vis)	Δδ (pH12.0-pH7.0) = 0.32	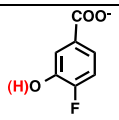
4F3HB:3HB6H	7.1 ± 0.2	Δδ (pH9.0-pH6.5) = 0.27	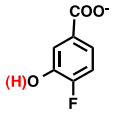
3F4HPA (without C_2)	9.03 ± 0.02 (4.21 ± 0.04)[a]	Δδ (pH10-pH6.6) = 0.20	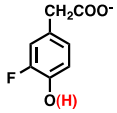
3F4HPA (Unbound to C_2)	8.9 ± 0.09	Δδ (pH10-pH6.6) = 0.16	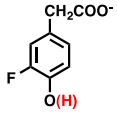
3F4HPA:C_2-WT	8.77 ± 0.03	Δδ (pH10-pH6.6) = -1.73	His120[b]
3F4HPA:C2-WT	p$K_{LH(EH)}$ = 6.2 ± 0.1 p$K_{(L)EH}$ = 8.1 ± 0.2 pK_{EH} = 7.1 ± 0.2 $K_{d,L•HE}$ = 25 ± 5 μM	fit to K_d *vs.* pH[e]	3F4HPA-O**H**•(EH) [b] His120im**H**•(L) [d] His120im**H** L•HE ⇆L^- + $^+$HE
3F4HPA:C2-WT	p$K_{LH(EH)}$ = 6.49±0.09 p$K_{LH(E)}$ = 7.5±0.5 p$K_{(L)EH}$ = 8.72±0.05 pK_{EH} = 7.7 ± 0.1 $K_{d,L•HE}$ = 38 ±6 μM	Simultaneous fit to Δδ and K_d *vs.* pH[e]	3F4HPA-O**H**•(EH) [b] 3F4HPA-O**H**•(E) [c] His120im**H**•(L) [d] His120im**H** L•HE ⇆L^- + $^+$HE
3F4HPA:C_2-S146A	8.8 ± 0.03	Δδ (pH9.8-pH5.8) = -1.63	His120im**H**•(L) [d]

[a] carboxyl of free 3F4HPA.
[b] (EH) indicates that the proposed nearby enzyme active site residue is protonated
[c] (E) indicates that the proposed nearby enzyme active site residue is not protonated
[d] (L) indicates that the deprotonated state of ligand is bound, and imH indicates deprotonation of the imidazolium side chain of His.
[e] Fixing pK_a of 9.0 for free 3F4HPA.

SCHEMES

Scheme 1.

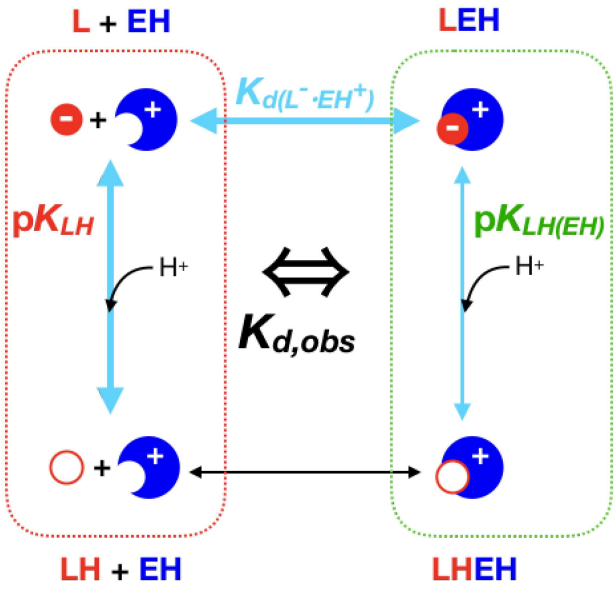

Scheme 2.

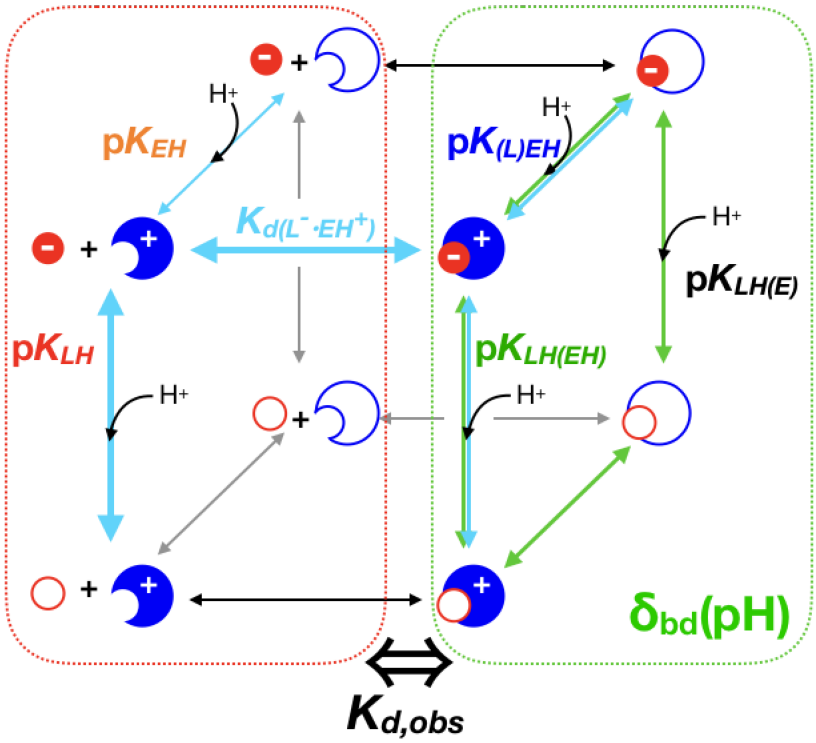

FIGURES

Figure 1.

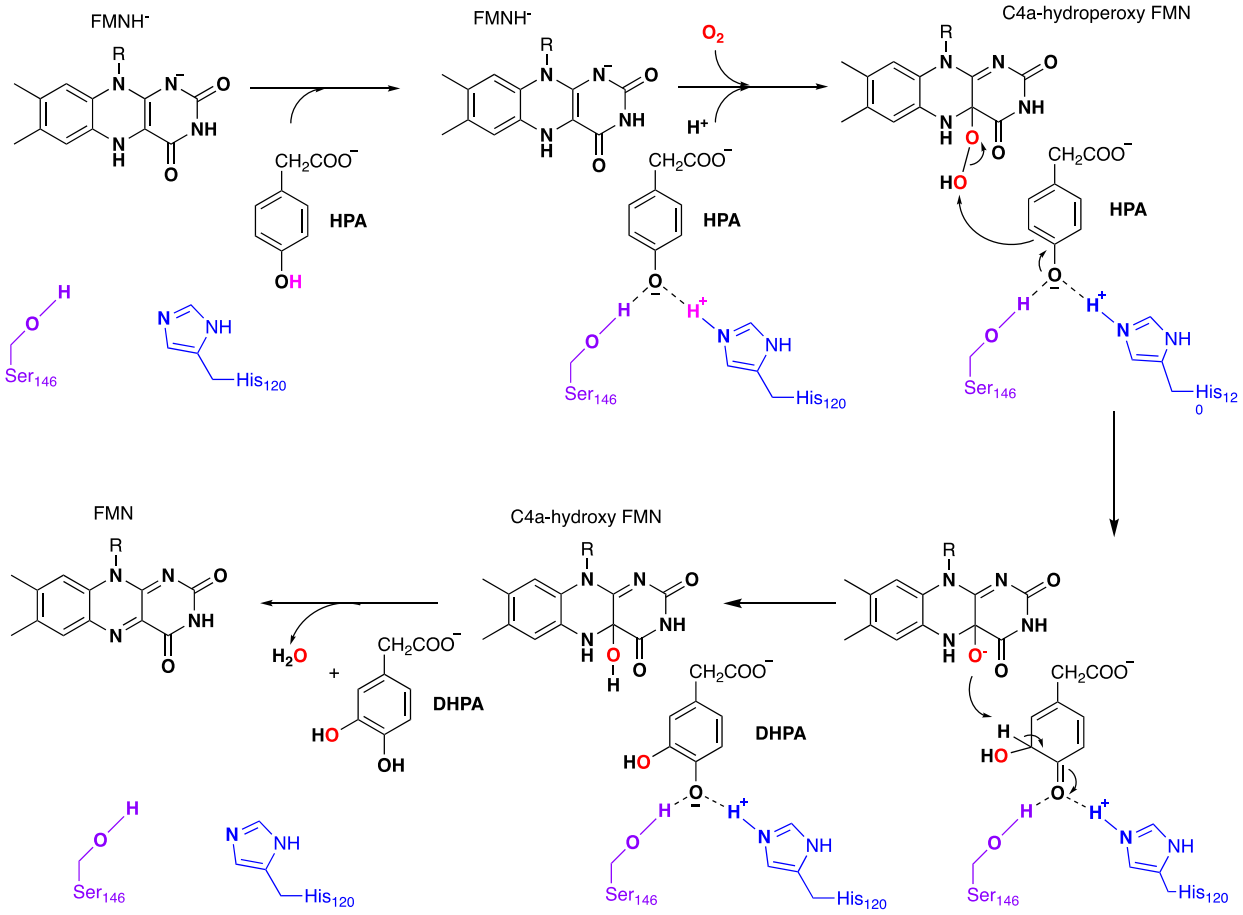

Figure 1. The proposed mechanism for electrophilic aromatic substitution as conducted by C_2 on its substrate 4HPA (11,36,37,74).

Figure 2.

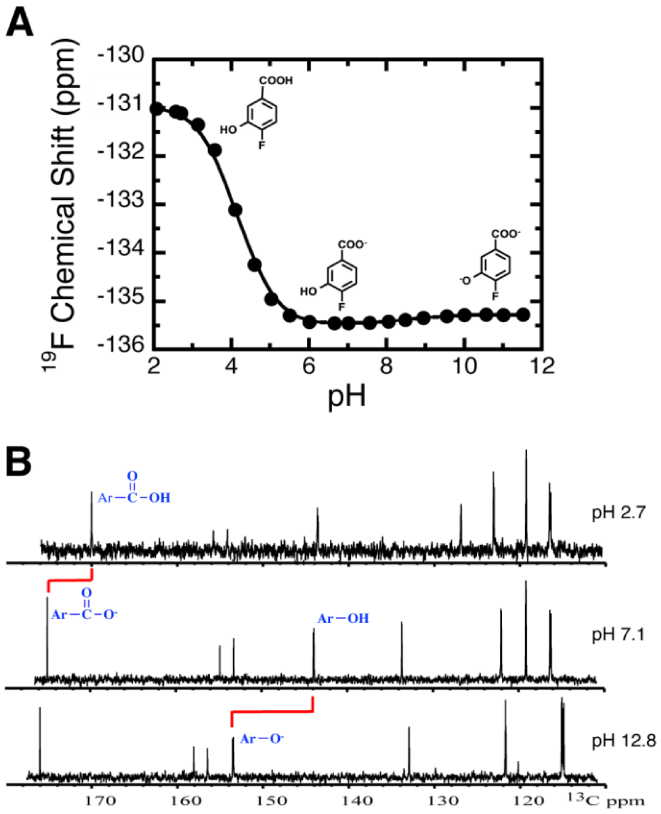

Figure 2. pH titration of the ^{19}F NMR chemical shift of 4F3HB. A: Fitting yielded pK_as of 4.1 ± 0.01 and 8.7 ± 0.03 for the carboxyl and phenol group, respectively. Structures of the ionization states of 4F3HB dominating in the three pH regions are shown, based on the data in B. B: ^{13}C NMR was used to identify the functional group whose ionization state changed with each pK_a. The carboxyl carbon near 180 ppm was most affected by changing pH from below to above the pK_a of 4.2 whereas the phenolic carbon that moves from near 146 ppm to near 156 ppm was most affected by changing the pH from below to above the pK_a of 8.7. Thus the data assign the pK_a of 4.1 to deprotonation of the carboxyl and the pK_a of 8.7 to deprotonation of the phenol. The signal near 135 ppm at pH 7.1 belongs to the C that subtends the carboxyl and the split signal near 160 ppm subtends the F.

Figure 3.

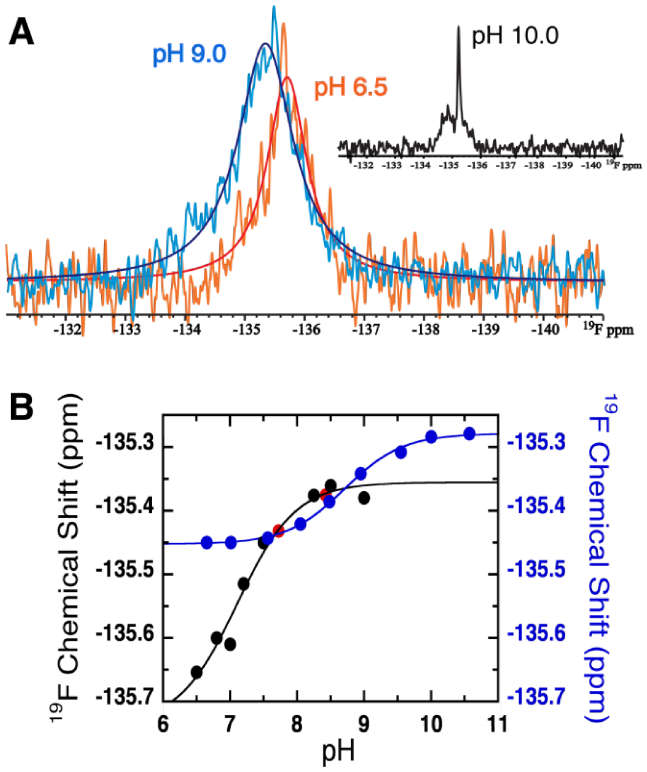

Figure 3. Effect of pH on the ^{19}F signal of 4F3HB in the presence of WT 3HB6H at 4 °C. (A) ^{19}F signal of 4F3HB bound to 3HB6H at pH 6.5 (orange spectrum) and pH 9.0 (light blue spectrum), the simulations of the NMR lines are shown in red and blue lines for the pH 6.5 and pH 9.0 spectra, respectively. Only bound ligand was observed from pH 6.0 to 9.0. However, the inset shows the ^{19}F spectrum at pH 10.0 showing the signal of free 4F3HB at -135.24 ppm in addition to the broader signal of bound ligand (see text). (B) Overlay of the pH titration curves obtained for bound 4F3HB in the presence of 3HB6H (black circles) and free 4F3HB in the absence of 3HB6H (blue circles). Red dots correspond to points in the back-titration, demonstrating excellent reversibility. The solid lines show the fits to the data of the Henderson-Hasselbalch equation (Eq. 3) to points acquired in the ascending titrations, which yielded pK_a values of 7.1 ± 0.2 (bound to 3HB6H) and 8.7 ± 0.03 (ligand alone).

Figure 4.

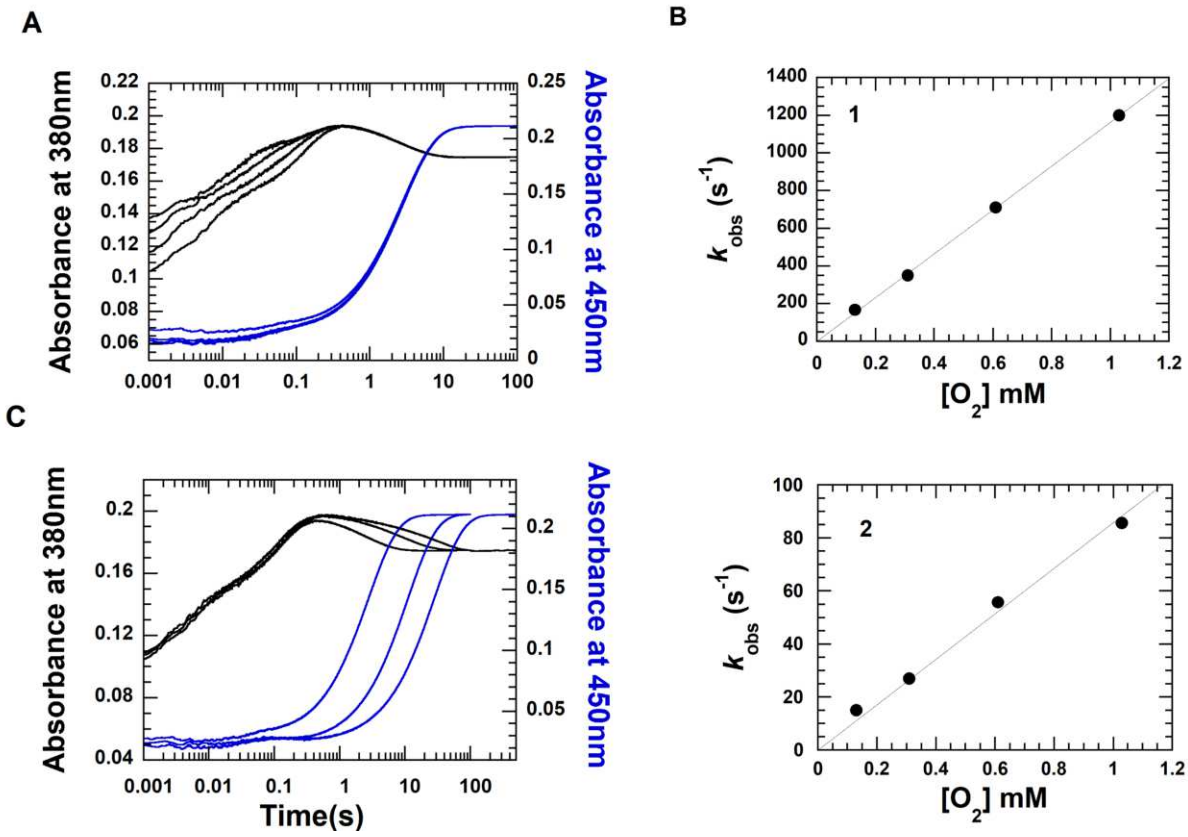

Figure 4. Reactions of C_2•FMNH$^-$ complex with O_2 in the presence of 3F4HPA. A) A solution of C_2 (100 μM), FMNH$^-$ (32 μM) and 2 mM 3F4HPA (before mixing) was mixed with buffers containing 2 mM 3F4HPA and various oxygen concentrations in a stopped-flow spectrophotometer. The reactions were monitored via the absorbance change at 380 and 450 nm (black and blue traces, respectively). Kinetic traces show four phases for A_{380}. The first and second phases are dependent on the oxygen concentration. (1.03, 0.61, 0.31 or 0.13 mM oxygen, respectively, was present for traces shown from left to right.) The black traces highlight formation then conversion of C4a-hydroperoxyflavin to C4a-hydroxyflavin and eventually to oxidized flavin. The third phase represents a slight increase in absorbance at 380 nm while the fourth phase is flavin re-oxidation (highlighted in blue traces). Both these phases are independent of oxygen concentration. (Compare with WT data in Figure 5 of (41).) B) Plots of k_{obs} of the first and second phases versus oxygen concentrations. Second-order rate constants for the first and second phases were calculated from the slopes of the plots to be 1.16 x 10^6 $M^{-1}s^{-1}$ (B, top) and 8.6 x 10^4 $M^{-1}s^{-1}$ (B, bottom), respectively. C) Reaction of C_2:FMNH$^-$ with oxygen and 3F4HPA at various concentrations. A solution of the reduced enzyme (C_2:FMNH$^-$) was mixed with buffer containing oxygen and various concentrations of 3F4HPA in a stopped-flow spectrophotometer. The reactions were monitored via the absorbance at 380 and 450 nm, as shown with black and blue traces, respectively. After mixing, the reaction contained C_2 (50 μM), FMNH$^-$ (16 μM), oxygen (0.13 mM) and various concentrations of 3F4HPA. The 450 nm kinetic traces reflect reaction with 2, 6, and 11 mM 3F4HPA respectively, from left to right.

Figure 5.

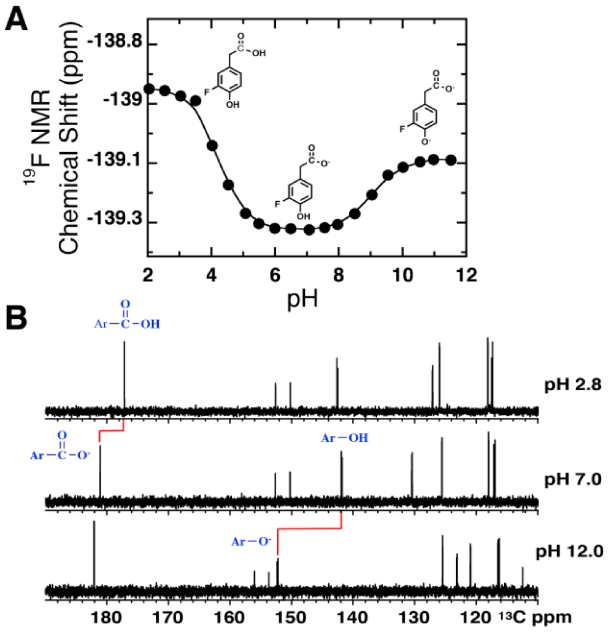

Figure 5. pH titration curves of 3F4HPA in the absence of wild-type C_2 at 25 °C. Panel A: The pH dependence of the ^{19}F chemical shift of 3F4HPA. Fitting to the Henderson-Hasselbalch equation (Eq. 3) yielded pK_as of 4.2 ± 0.04 and 9.0 ± 0.02 for the carboxyl and hydroxyl group, respectively. Structures of the ionization states of 3F4HPA dominating in the three pH regions are shown, based on the data in panel B. Panel B: ^{13}C NMR determination of the events responsible for the different pK_as. The carboxyl carbon near 180 ppm is most sensitive to the pK_a of 4.2 whereas the phenolic carbon near 140 ppm (at pH 7.0) is most sensitive to the pK_a of 9.0.

Figure 6.

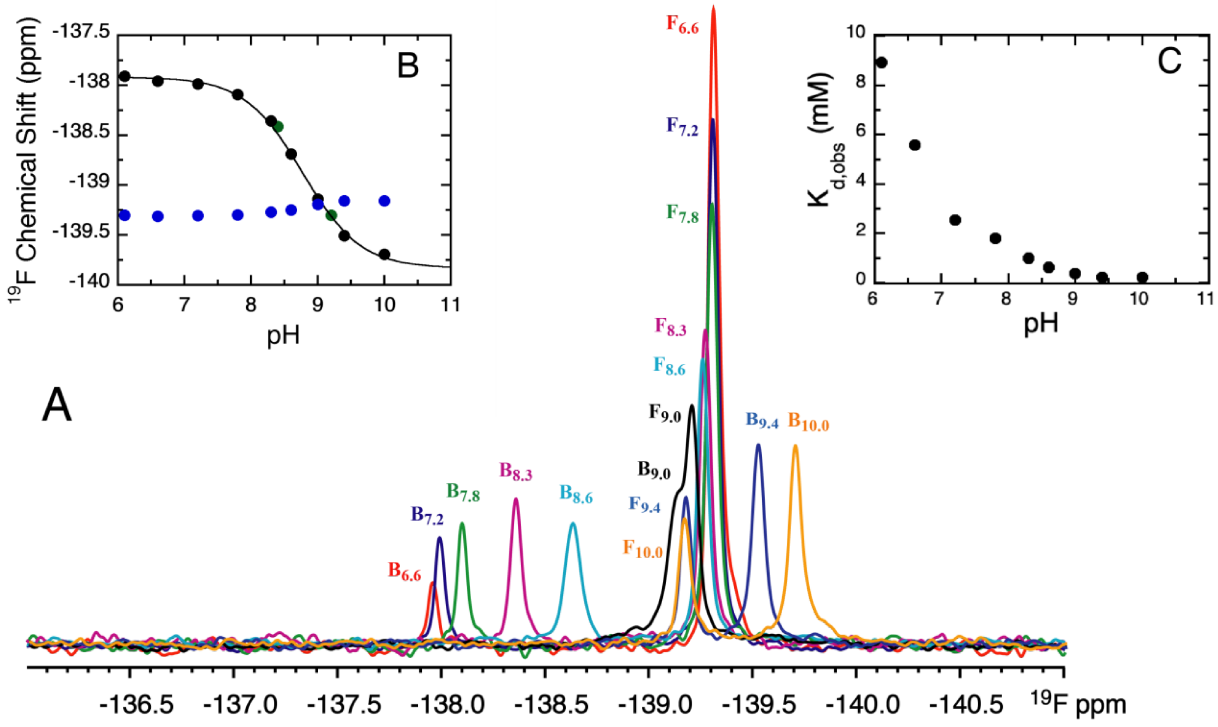

Figure 6. Effect of pH on the ^{19}F signal of 3F4HPA free or bound to wild-type C_2•FMNH$^{\cdot}$. (A) The ^{19}F spectrum of 3F4HPA at a series of pHs show both bound (B) and free (F) 3F4HPA in the presence of WT C_2 and FMNH$^{\cdot}$. pHs reported are pH 6.6 (red spectrum), pH 7.2 (blue spectrum), pH 7.8 (green spectrum), pH 8.3 (magenta spectrum), pH 8.6 (cyan spectrum), pH 9.0 (black spectrum), pH 9.4 (light blue spectrum), and pH 10.0 (orange spectrum). All spectra are presented using the same vertical scale, and were collected at 25 °C. Inset (B) shows the pH dependence of the ^{19}F shifts of 3F4HPA bound to C_2 (black circles) or free (blue circles). The green circles represent data from back-titration and demonstrate reversibility. The solid line provides the fit to the data of the Henderson-Hasselbalch equation (Eq. 3) with pK_a = 8.7 ± 0.03, for bound 3F4HPA. For free 3F4HPA a pK_a of 8.9 ± 0.09 was obtained (curve not shown). Inset (C) plots the observed dissociation constants vs the sample pH documenting tighter binding at higher pH, as predicted for favorable interaction between the phenolate form of substrate and a cationic protein site. All data were collected under inert atmosphere.

Figure 7.

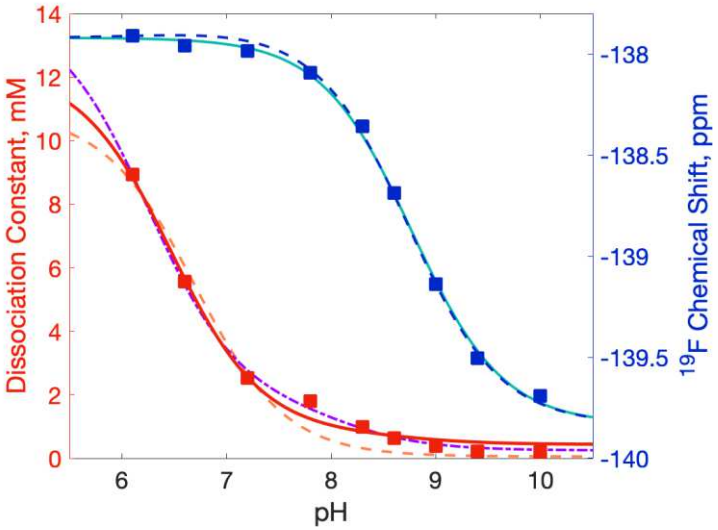

Figure 7. Application of Model 2 to the pH dependence of the ^{19}F chemical shift (blue squares) and the observed dissociation constant (red squares) of 3F4HPA binding to wild-type C_2. Dissociation constants determined at different pHs using Eq. 2 are plotted against pH values (red squares) and compared with the predictions of the different models. Model 1 (Scheme 1) produced the fit shown with the orange dashed line obtained using Eq. 1 which yielded a high-pH limiting dissociation constant of 0.05 ± 0.01 mM for the L•EH complex and a $pK_{LH(EH)}$ of 6.7 ± 0.1, using the free ligand pK_a of 9.0. This model provided an inadequate description of the data near pH 8.0 and so was replaced by the two-proton model (Scheme 2). The resulting fit to the data using Eq. 5 better reproduced the intermediate-pH behavior (dot-dashed purple line) and yielded a limiting $K_{d,L•EH}$ of 0.025 ± 0.005 mM, pK_{EH} of free enzyme of 7.1 ± 0.2, $pK_{LH(EH)}$ for ligand bound to protonated enzyme of 6.2 ± 0.1, $pK_{(L)EH}$ for enzyme with deprotonated ligand bound of 8.1 ± 0.2. The pH dependence of the chemical shift was well described by the Henderson-Hasselbalch equation Eq. 3, yielding a pK_a of 8.77 ± 0.03 (teal line). When the chemical shift and $K_{d,obs}$ were fit simultaneously in Matlab the intermediate pH behavior of $K_{d,obs}$ was not as well described (red solid line), but the parameters obtained from the simultaneous fit are comparable to those obtained from fits to each of chemical shift and $K_{d,obs}$ alone, and the chemical shift's pH dependence was quite well described (blue dashed line). Obtained parameters are provided in Table 2.

Figure 8.

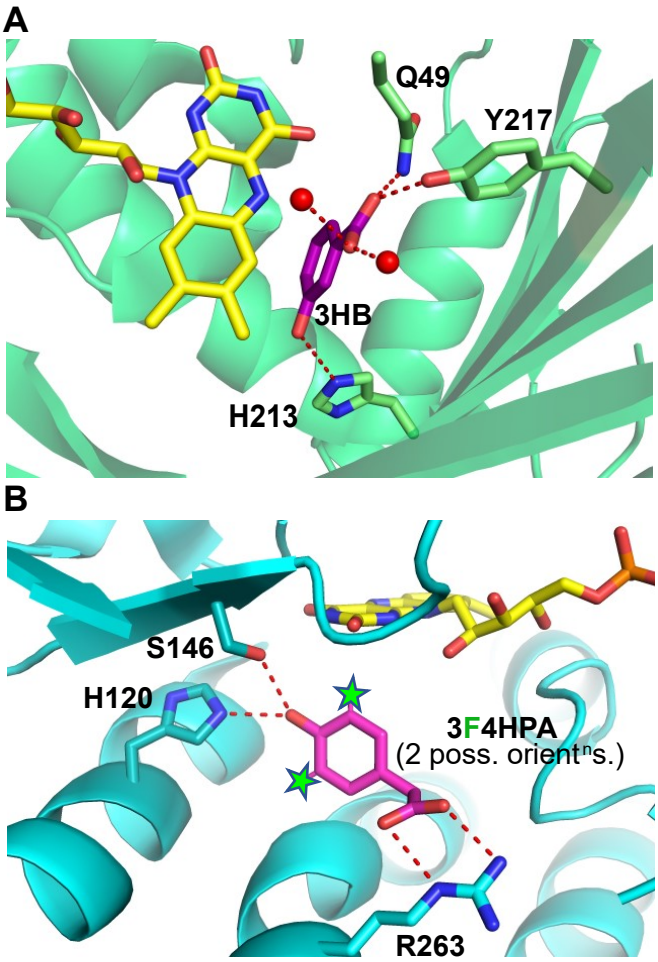

Figure 8. Ribbon structures of (A) the active site of 3HB6H bound with 3HB bound and (B) the active site of WT-C_2 with 4HPA bound and the two positions F can occupy indicated by stars. The 3HB6H structure was obtained by co-crystallization of the His213Ser variant of 3HB6H with 3HB (4BK1.pdb) (53). UCSF's Chimera program (75) was used to model the WT His residue in place of Ser213. The rotamer of His213 that best overlays the Ser residue and approaches bound substrate without production of clashes was selected and the energy of the resulting structure was minimized within Chimera. In (B) the active site of WT-C_2 co-crystalized with 4HPA is shown (2JBT.pdb (49)). To show the locations that could be occupied by F atoms when 3F4HPA is bound, we designated both the 3 and 5 Hs of the 4HPA ligand as F atoms and identified them with stars to underscore that they are not experimentally determined F positions. Although the substrate analog we used has F in only one position, we do not know which of two possible orientations it might prefer when bound, or whether both orientations are populated. Thus, the two 'F's in the figure represent two possible positions of F, neglecting additional possible effects of enzyme dynamics. One of these positions is consistently ≈ 4 Å from the Nε of His 120 in our model active sites.

Figure 9.

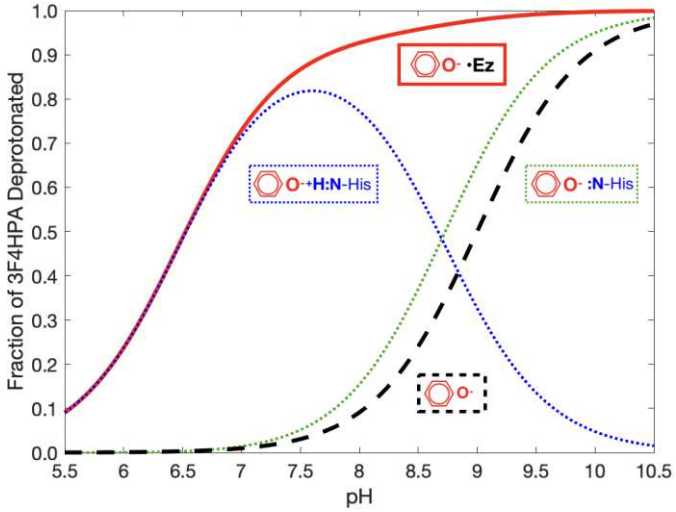

Figure 9. Extent of deprotonation of 3F4HPA free or bound to wild-type C_2•$FMNH^-$ as a function of pH. The extents to which the two different states containing deprotonated 3F4HPA are populated (dotted lines), along with the total extent to which 3F4HPA is deprotonated (solid red line), based on our model and the pK_a values that emerged from our fits to the data. At high pHs above 8.7, the active site His120 and bound 3F4HPA are both predominantly deprotonated (dotted green). At lower pHs where free 3F4HPA would normally be protonated (dashed black), the protonated state of His120 stabilizes **de**protonated 3F4HPA (dotted blue). Thus, our model indicates that enzyme-bound substrate is deprotonated to a much lower pH than free substrate (red curve vs. dashed black), and that the enlarged pH span for the substrate phenolate is due to cationic His120 (dotted blue). Our data thereby predict a substantially pH independent catalytic rate over the pH range of 6.5 to 10.